




## Article

# Chronological and Archaeometric Evaluation of Bricks from Archaeological Sites of Upper Assam, Northeast India: Estimation of the Firing Temperature and Civilization History

Raktim Ranjan Saikia <sup>1</sup>, Chaitra Dhar Taye <sup>1</sup>, Nurul Amin <sup>1</sup>, Sorat Konwar <sup>1</sup>, Laura Panzeri <sup>2,\*</sup> and Anna Galli <sup>2</sup>

<sup>1</sup> Department of Geology, Jagannath Barooah College, Jorhat 785001, India; raktimrsaikia@gmail.com (R.R.S.); chaitradhar2010@gmail.com (C.D.T.); naminjbc@gmail.com (N.A.); soratkonwar770@gmail.com (S.K.)

<sup>2</sup> Dipartimento di Scienza dei Materiali, Università degli Studi di Milano-Bicocca, Via R. Cozzi 55, 20125 Milano, Italy; anna.galli@unimib.it

\* Correspondence: laura.panzeri@unimib.it

**Abstract:** This study aimed to uncover the chronology and production technologies of ancient bricks unearthed from various locations in Upper Assam, Northeast India. To achieve this goal, complementary spectroscopic techniques such as Fourier Transform Infrared Spectroscopy (FTIR), X-ray Diffraction (XRD), Scanning Electron Microscope (SEM) coupled with Energy Dispersive Spectrometer (EDS), as well as Thermoluminescence (TL) and Optically Stimulated Luminescence (OSL/IRSL) dating, were applied. FTIR and XRD analyses revealed the presence of quartz, feldspar (microcline, orthoclase, albite), kaolinite, chlorite, cerussite, palygorskite, magnetite, hematite, and organic carbon. The mineralogical composition indicates two distinct groups with firing temperatures below 650 °C and above ~800 °C. These two groups could be the first indication of the presence of two civilizations or at least two different production technologies involving different firing temperatures and kiln atmospheric conditions. Further, the SEM-EDS study suggests that both calcareous and non-calcareous clays were used in brick making, which have low and high refractory properties, respectively. The internal morphology of the samples shows the existence of micropores and microfractures, indicating the influence of higher-temperature firing. Absolute dating techniques associate the two brick groups with different age ranges: a firing temperature above ~800 °C indicates a superior technology corresponding to a production period between the 7th and 10th centuries CE. In contrast, a temperature below 650 °C indicates a technologically less advanced group of people, with the age group dated between the 11th and 14th centuries CE.

**Keywords:** firing temperature; XRD-FTIR; SEM-EDS; archaeometry; ancient bricks; TL/OSL dating



**Citation:** Saikia, R.R.; Taye, C.D.; Amin, N.; Konwar, S.; Panzeri, L.; Galli, A. Chronological and Archaeometric Evaluation of Bricks from Archaeological Sites of Upper Assam, Northeast India: Estimation of the Firing Temperature and Civilization History. *Appl. Sci.* **2024**, *14*, 6271. <https://doi.org/10.3390/app14146271>

Academic Editor: Syed Minhaj Saleem Kazmi

Received: 11 June 2024  
Revised: 1 July 2024  
Accepted: 12 July 2024  
Published: 18 July 2024



**Copyright:** © 2024 by the authors. Licensee MDPI, Basel, Switzerland. This article is an open access article distributed under the terms and conditions of the Creative Commons Attribution (CC BY) license (<https://creativecommons.org/licenses/by/4.0/>).

## 1. Introduction

The history of human civilization is inherently connected to the use of bricks as a basic building material. Since the third century BCE, there have been numerous structures that use fired or burned bricks [1]. The chronicles of ancient civilizations give evidence to the enduring legacy of brick creation, and several studies infer that the quality and durability of bricks are closely related to the quality of raw materials, manufacturing techniques such as firing temperature, and many other factors [2–5]. Firing temperature is recognized as an important factor in brick production because burning triggers significant changes in mineralogy, texture, and physical properties, impacting the porosity and pore dispersion of bricks [6–9].

When clays are fired to make pottery, new minerals called firing minerals are formed. These products are primarily determined by the composition of the clays, the additives used to make pottery, the atmospheric conditions, and the duration of firing during pottery making. Gehlenite and diopside are high-temperature firing minerals. Gehlenite is formed at 800–850 °C as illite and calcite decomposition products [10]; calcite decomposition begins at 650 °C and ends at 850 °C, generating new high-temperature calc-silicates and

aluminum–calcium silicates such as pyroxene group members (diopside) and plagioclase feldspars (anorthite) [11,12]. The reaction between quartz and lime at 920 or 1000 °C, depending on the quartz content, produces wollastonite. Wollastonite was discovered to replace gehlenite in the gehlenite bearing system at temperatures above 830 °C [13]. Multidimensional approaches like X-ray powder Diffraction (XRD), Fourier Transform Infrared Spectroscopy (FTIR), Differential Thermal Analysis (DTA), and Scanning Electron Microscopy (SEM) have been demonstrated to be very effective for understanding the firing temperature [5,14–19]. Moreover, the Thermoluminescence (TL) and Optically Stimulated Luminescence (OSL) dating techniques are essential for establishing the time elapsed since the last high-temperature event, which usually coincides with the bricks' firing in a kiln [20,21]. TL and OSL exploit the accumulation of charge carriers in mineral defects, providing a timeline for brick usage and reuse [22,23].

In India, most investigations have focused on the ancient architectures of the Southern part of the country, using similar methodologies to understand the effects of firing temperature and the physical-mechanical properties of ancient bricks [19,24–31]. However, only one notable study analyzed the bricks of the Kamakhya Temple using XRD and FTIR techniques, revealing variations in firing temperatures (above and below 500 °C) [32]. Except for this, no archaeometric and dating studies of ancient artifacts from the region have been carried out so far. Hence, the present study aimed to fill this gap by focusing on different archaeological sites of Upper Assam to estimate technological parameters of brick production, such as raw materials and the firing temperature used in manufacturing, employing FTIR, XRD, and SEM-EDX techniques. Additionally, TL, OSL, and IRSL dating methods were employed to determine the chronology and historical context of the Dihing Valley and nearby areas of Upper Assam. In this way, it was possible to establish whether different brick production technologies exist and, thanks to the determination of an absolute chronology, determine the technological progress that has occurred in brick production.

### 1.1. Study Area

In recent years, a few important archaeological structures framed with bricks were noticed in four archaeological sites in Upper Assam (Figure 1). The locations and details of the archaeological sites are described below.

#### 1.1.1. Mouramora Archaeological Spot

Mouramora is situated on the bank of a palaeo-channel of the River Dihing of the Dibrugarh district in Assam, India, at a latitude of 27°20'7.051" and a longitude of 94°55'45.512". It was excavated by the Archaeological Survey of Assam in 2017. The unearthed structure looks like the plinth of an old temple, maybe constructed on the bank of the old River Dihing, now found as a palaeo-channel of it (Figure 2a). The structure is built with bricks of different shapes and sizes, with sharp and curved edges (Figure 2b). The sizes range from 30 cm × 21 cm to about 15 cm × 15 cm, with a thickness of about 5 cm. The morphology of the structure and its structural arrangement indicate that it was prepared by a well-organized group of people. A total of three samples of different shapes and sizes have been collected from the site for this work.

#### 1.1.2. Pratima Garh Archaeological Spot

Pratima Garh is a square-shaped defensive barricade located in the Sadiya of the Tinsukia district in Assam, India, at a latitude of 27°54'41.400" and a longitude of 95°41'25.500". The length of the side of the barricade measures almost 300 m. There is an almost 4.5 m high central mound structure (Figure 2c). Although the site is still not excavated, one brick sample from this central mound was collected for the present study (Figure 2d,e).

#### 1.1.3. Padum Pukhuri Archaeological Spot

The studied location is situated in Sadiya near the Assam-Arunachal state border, India, at a latitude of 27°57'48.110" and a longitude of 95°45'40.000". It is an ancient

tank with a bank fortified with bricks. It is a square-shaped dry tank structure. The recently measured depth of the tank is 3 m, and the length of the side is 150 m (Figure 2f). Systematic excavation of this pond has not yet started. The brick sample investigated here was collected from the bank of the tank (Figure 2g,h).

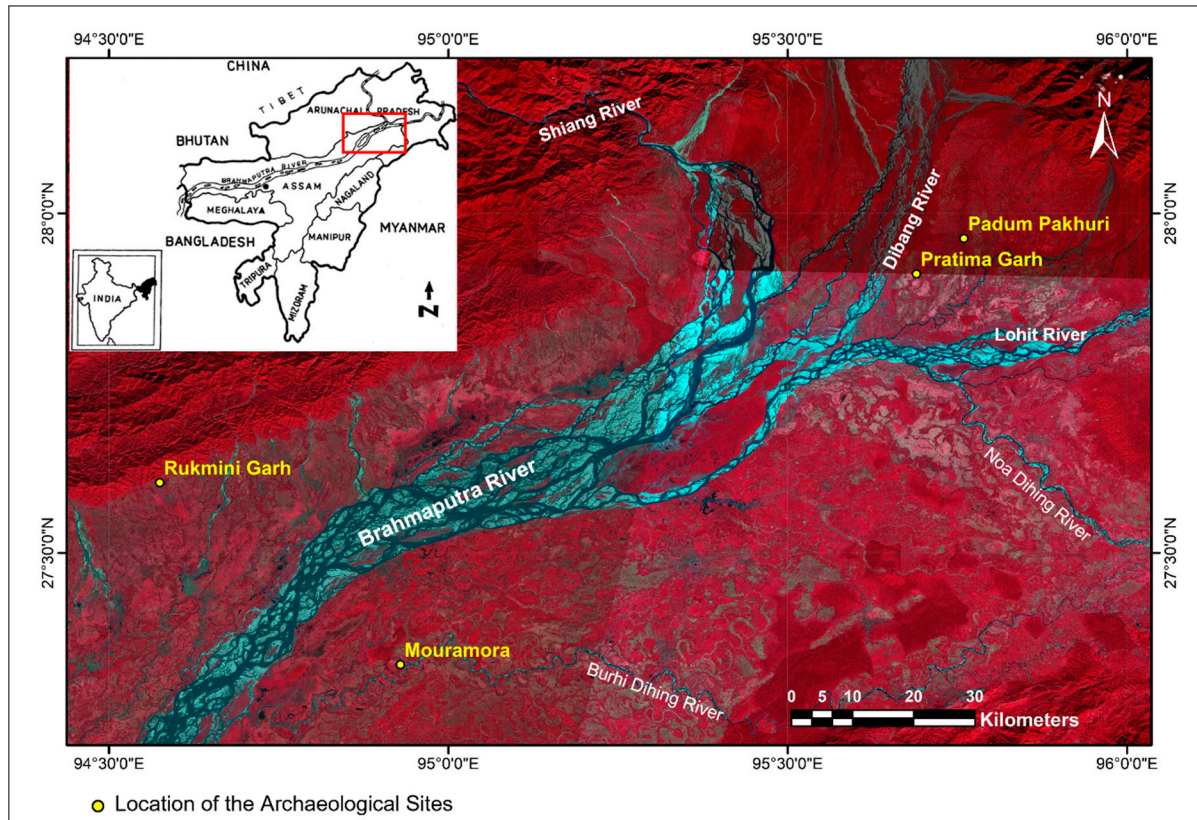


**Figure 1.** Location map of the study area indicating archaeological sites. The red rectangle in the map indicates the study area.

#### 1.1.4. Rukmini Garh Archaeological Spot

Rukmini Garh is positioned in the Dhemaji district of Assam, India, at a latitude of  $27^{\circ}36'11.933''$  and a longitude of  $94^{\circ}34'28.817''$ . It is a 550 m (as preserved today) long defensive embankment, starting from the foothills of the Eastern Himalayan (Arunachal-Himalaya) region and aligned along a North–South direction (Figure 2i). It is assumed that it was originally much longer in length, but due to the seasonal floods of the Jokai River (neighboring river), only a 550 m long area remains, although in poor condition. The construction pattern of the structure is uncommon. At first, a core brick wall was constructed, and the wall was covered with a thick cover of soil. The core brick wall and the soil cover combined made a strong defensive embankment. Samples from the core of the embankment were collected for the study (Figure 2j). This place has not been excavated yet.



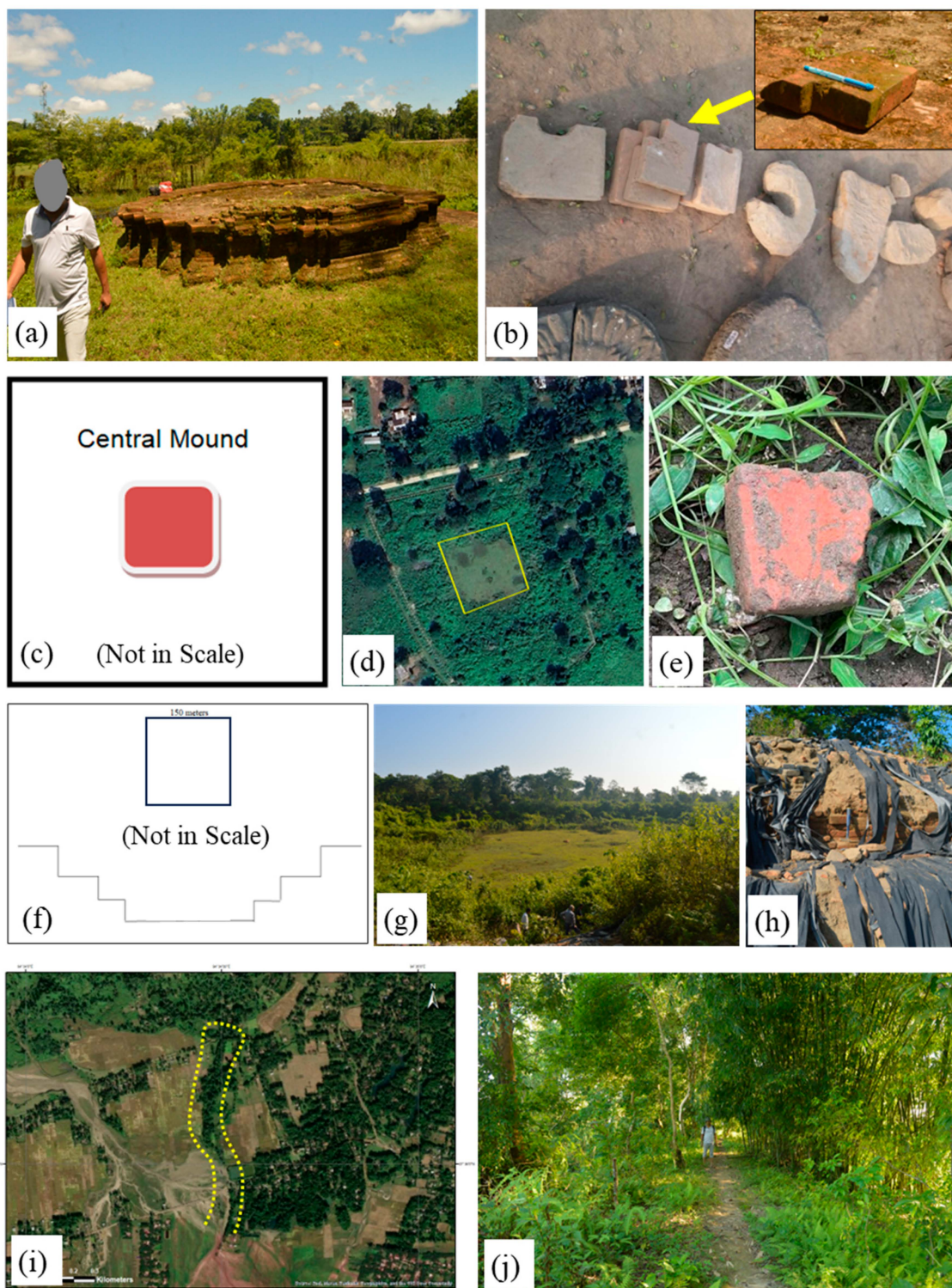


**Figure 2.** Representative field photograph of four archaeological sites. (a) Plinth-like old temple structure of Mouramora; (b) Flat and varied shaped bricks used to make the plinth-like structure of Mouramora; The yellow arrow indicates bricks with a sample in the inset, where a pen ~15 cm in length is used as scale; (c) Sketch of the sample point of central mound structure of ancient Pratima Garh; (d) Satellite image representing remnants of central mound structure of ancient Pratima Garh; (e) Close up view of collected samples of Pratima Garh; (f) Top view sketch and cross-sectional profile of the ancient tank of Padum Pukhuri; (g) Field photographs showing vegetation-covered Padum Pukhuri and (h) Intake bricks on the bank of Padum Pukhuri; (i) Satellite image representing remnants of long defensive embankment of Rukmini Garh; and (j) Field photographs of poorly preserved ancient embankment of Rukmini Garh.

## 2. Materials and Methods

To achieve the goal of the present study, six brick samples were collected from the specified archaeological sites in Upper Assam (three from Mouramora and one from the Pratima Garh, Rukmini Garh, and Padum Pukhuri sites). The collected samples were studied systematically using the following procedures.

### 2.1. Color of the Bricks Identification

The color of the bricks was identified using the Munsell color chart, 1994 revised edition. All the samples from the Mouramora site, called Mouramora 1, 2, and 3, show a light red color (7/6, HUE 2.5 YR). Other samples, such as those from Padum Pukhuri, Rukmini Garh, and Pratima Garh, display light red (6/6, HUE 10R), reddish-yellow (6/6, HUE 5 YR), and weak red (5/4, HUE 10R) colors, respectively (Figure 3).

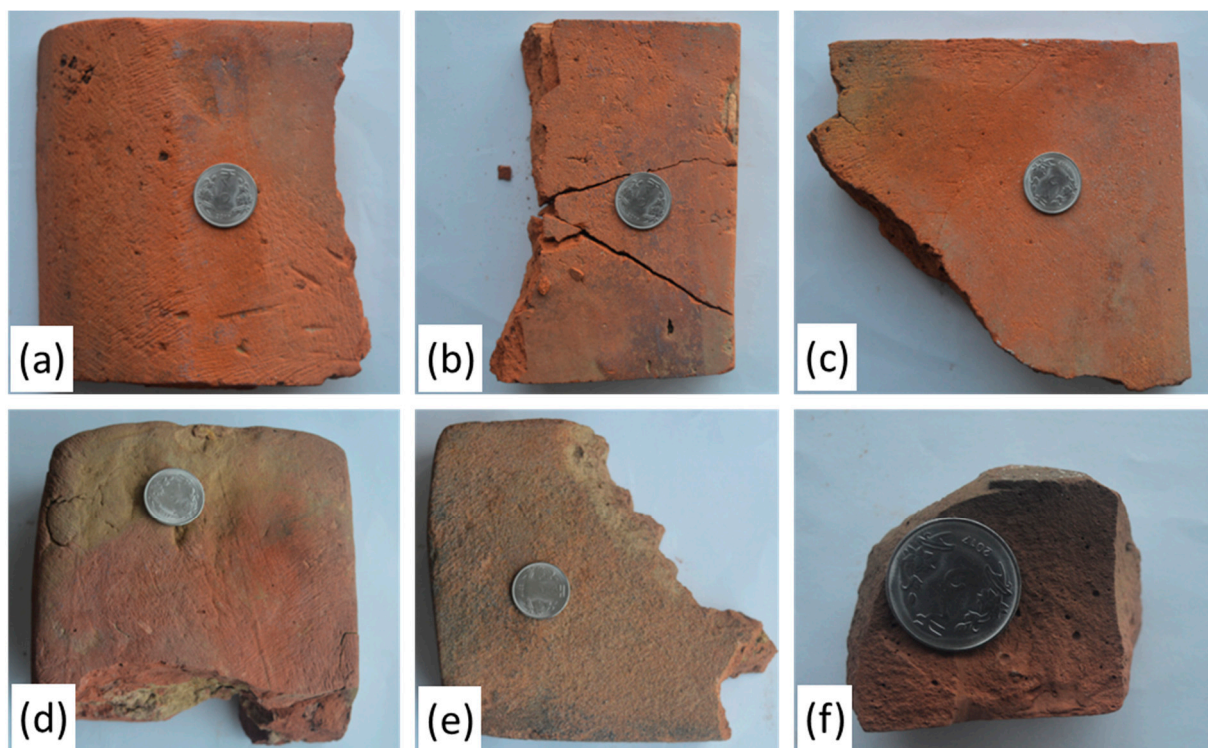


**Figure 3.** Photograph representing the color of the bricks of four archaeological sites: (a–c) the Mouramora site, (d) Padum Pukhuri, (e) Rukmini Garh, and (f) Pratima Garh. Coins with a diameter of ~2 cm are used as reference.

### 2.2. XRD and FTIR Analysis

A small portion of the samples was thoroughly grinded using an agate mortar to make a fine powder for XRD and FTIR analyses. The XRD analysis was carried out using an ULTIMA IV (Rigaku, Japan) X-ray diffractometer with  $\text{CuK}\alpha$  radiation in  $2\theta$  mode between  $2^\circ$  and  $80^\circ$  with  $\pm 2\%$  basic accuracy. The mineral phases present in the studied bricks were identified after comparing their d-spacing and  $2\theta$  values in the published literature [33–35].

The FTIR spectra of the samples were determined after being pelletized with spectra grade KBr and recorded at room temperature in a wide range of wave numbers from  $400$  to  $4000\text{ cm}^{-1}$  by using a FTIR-SPECTRUM two (Perkin Elmer Inc., Waltham, MA, USA) spectrometer. XRD and FTIR analyses were carried out at the CSIR-North East Institute of Science & Technology, Jorhat, India.



### 2.3. SEM and EDS Analysis

To investigate the internal morphology of the brick samples, they were analyzed using Scanning Electron Microscopy (SEM) and Energy Dispersive Spectrometer (EDS) techniques. SEM, coupled with the elemental analysis, was conducted using a Field Emission Scanning Electron Microscopy (FESEM) produced by Carl ZEISS Microscopy, Germany. The samples, coated with a thin layer of gold or platinum, were examined with SEM, using various magnifying powers for all the samples in the study. The investigation of SEM and EDS analyses of the studied brick samples was performed at the CSIR-North East Institute of Science & Technology, Jorhat, India.

### 2.4. TL and OSL/IRSL Dating

For the TL and OSL/IRSL dating investigation, the material was sampled with a low-speed drill from the inner part of the bricks, and all the procedures were followed under dim red light according to the fine-grain protocol [36]. The obtained polymineral fraction (4–11  $\mu\text{m}$ ) was settled onto stainless steel discs and used for both TL and OSL/IRSL measurements. This fraction, mainly consisting of quartz and feldspars, can be excited using both blue (OSL) and infrared radiations (IRSL), the latter being effective only on feldspars.

TL/OSL/IRSL measurements were performed with a Risø TL-DA-20 reader, using blue-LEDs ( $470 \pm 30 \text{ nm}$ ,  $\sim 72 \text{ mW/cm}^2$ ) for OSL and infra-red LEDs ( $\lambda = 850 \text{ nm}$ ,  $\sim 270 \text{ mW/cm}^2$ ) for IRSL, detecting the emitted photons with an Electron Tube PDM 9107Q-AP-TTL-03, coupled with a U-340 filter for OSL and a Schott BG3/BG39 filter combination for IRSL measurements. The system is equipped with an internal  $^{90}\text{Sr}$ - $^{90}\text{Y}$  beta source (dose rate:  $0.127 \pm 0.05 \text{ Gy/s}$ ).

To evaluate the Equivalent Dose (E.D.), two different techniques were applied: the Multiple-Aliquot Additive protocol (MAAD, Aitken [20] was used for TL, and the Single Aliquot Regenerative dose (SAR, ref. [37] protocol was used for OSL and IRSL.

The annual dose rate was indirectly derived from the measurement of the radioactivity of the samples. The U and Th concentrations were obtained with total alpha counting using ZnS scintillator discs, assuming a Th/U concentration ratio equal to 3.16 (Aitken, 1985). The contribution due to  $^{40}\text{K}$  content was deduced from the total concentration of K obtained using flame photometry. For IRSL, the effect of the internal K-content of feldspar was considered. Alpha particles are less effective in inducing luminescence than beta and gamma radiation. This was considered introducing the  $a$ -value determination, which is based on the comparison of the luminescence signals induced by alpha and beta laboratory irradiations. Because water absorbed part of the radiation that would otherwise reach the sample, the saturation water content was evaluated for each brick. The  $F$  value (i.e., the fraction of saturation to which the assumed average water content corresponds) was considered equal ( $75 \pm 10$ )% for all samples, considering the available information on humidity in the area. The cosmic rays' contribution to the final dose rate was added [38]. The TL/OSL/IRSL dating was performed in the LAMBDA Lab of the Department of Material Science of the University of Milano-Bicocca, Milano, Italy [39].

## 3. Results and Discussion

In the following sections, the obtained data are discussed.

### 3.1. Identification of Minerals through FTIR Analysis

The FTIR spectra of the studied brick samples are depicted in Figure 4a. Since a few FTIR spectra are not easy to interpret on a whole-range scale, the graphs were separated into two ranges spanning  $1200\text{--}400 \text{ cm}^{-1}$  and  $4000\text{--}3000 \text{ cm}^{-1}$  (Figure 4b,c). The minerals identified in the spectra were based on existing literature sources (listed in Table 1). They include quartz, feldspar (albite, orthoclase), kaolinite, palygorskite, chlorite, organic carbon, cerussite, hematite, and magnetite. All the brick samples under investigation contain quartz, kaolinite, organic carbon, and palygorskite (barring Rukmini Garh).

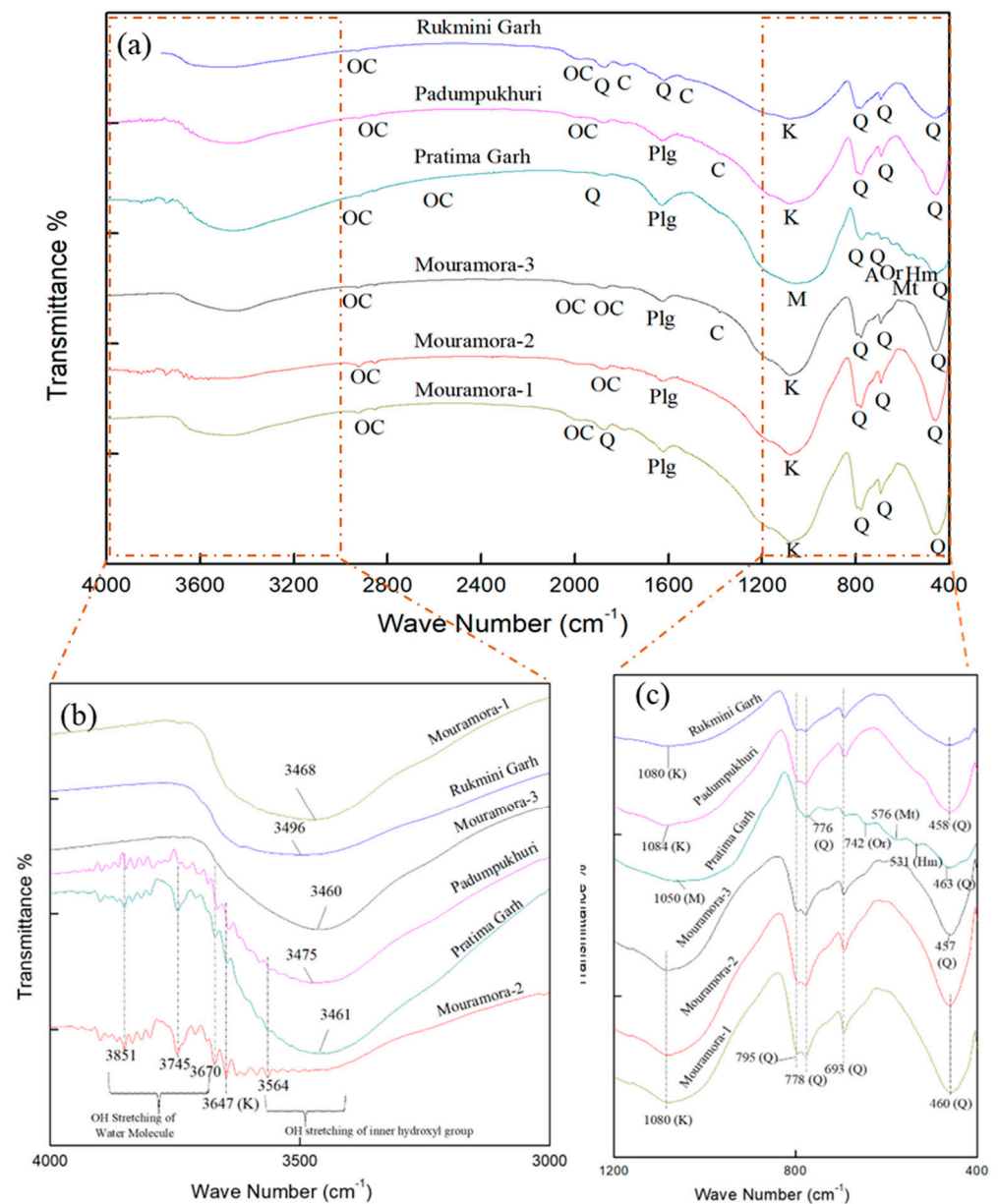


**Figure 4.** FTIR spectrum of studied brick samples: (a) FTIR spectrum ranges from 4000–400  $\text{cm}^{-1}$ , (b) FTIR spectrum ranges from 4000–3000  $\text{cm}^{-1}$ , and (c) FTIR spectrum ranges from 1200–400  $\text{cm}^{-1}$  (Q—Quartz, Or—Orthoclase, A—Albite, Mt—Magnetite, Hm—Hematite, K—Kaolinite, Plg—Palygorskite, C—Carbonates, Ch—Chlorite, OC—Organic Carbon).

The presence of quartz was confirmed by characteristic vibrational peaks at 457–458  $\text{cm}^{-1}$  (Si-O asymmetrical bending), 460–463  $\text{cm}^{-1}$  (Si-O asymmetrical bending), 692–693  $\text{cm}^{-1}$  (Si-O symmetrical bending), and 776–778 and 795  $\text{cm}^{-1}$  (Si-O symmetrical stretching). The existence of quartz in the Mouramora-1, Pratima Garh, and Rukmini Garh brick samples was supported by the presence of weak absorption peaks at 1619  $\text{cm}^{-1}$  and 1870–1876  $\text{cm}^{-1}$ .

The feldspar group of minerals is merely present in the Pratima Garh brick sample, which included orthoclase, microcline (K-feldspar), and albite (Na-feldspar). Their presence was established by identifying the vibrational peaks at 1050  $\text{cm}^{-1}$  (Si-Al-O stretching for microcline feldspar), 642  $\text{cm}^{-1}$  (Al-O coordination vibrations suggesting orthoclase feldspar), and 725  $\text{cm}^{-1}$  (Al-O-Si stretching for albite feldspar).

In general, four significant IR spectra of OH-stretching regions are employed to distinguish kaolinite, with relative intensities of 3695, 3665, 3650, and 3620  $\text{cm}^{-1}$  [40,41]. However, the presence of other minerals may influence the intensity and resolution of

these vibration bands. The studied samples encompass no prominent kaolinite peaks at the expected values. In Ref. [41] the authors assigned the OH stretching region peak with an intensity of  $3647\text{ cm}^{-1}$  as kaolinite. Under this assumption, the presence of this peak with weak OH stretching of the inner hydroxyl group in the Mouramora-2 and Pratimagarh samples confirms the signatures of kaolinite. The spectra region from  $3671$  to  $3851\text{ cm}^{-1}$  represents the OH stretching of water molecules. The  $3460$ – $3496\text{ cm}^{-1}$  spectra imply mixed layered OH stretching and bending vibrations of inner-surface hydroxyl groups. The OH stretching of the inner hydroxyl group chlorite mineral was also observed in the Mouramora-2 samples at  $3565\text{ cm}^{-1}$ . The IR spectrum for kaolinite with thin particles exhibits peaks at  $1105$  and  $695\text{ cm}^{-1}$ ; however, as the particle size increases, the vibrational bands shift to  $1080$  and  $689\text{ cm}^{-1}$  [40]. Barring the sample Padumpukhuri, the other samples display broadening bands at  $1080$  and  $1084\text{ cm}^{-1}$ .

Carbonate minerals have been found in three different samples: Mouramora-3, Padum Pukhuri, and Rukmini Garh, with FTIR peaks at  $1381$ ,  $1384$ , and  $1788\text{ cm}^{-1}$ . The mineral with a prominent relative intensity at  $1396\text{ cm}^{-1}$  was identified as cerussite [42]. However, Ramasamy et al. [28] also considered the peaks at  $1380$ – $1385\text{ cm}^{-1}$  as indicative of cerussite. Hence, the presence of spectra at  $1381$ ,  $1384$ , and  $1788\text{ cm}^{-1}$  is in good agreement with the carbonate minerals cerussite and calcite, respectively.

The complex nature of absorption bands in stretching and bending regions of water molecules is characteristic of palygorskite. Palygorskite may be responsible for the presence of bands in the region of  $1623$ – $1630\text{ cm}^{-1}$ . Many researchers have studied similar patterns [43–45].

An additional peak in the ranges of  $2919$ – $2928$ ,  $2851$ – $2854$ ,  $2004$ ,  $1984$ – $1998$ , and  $1878$ – $1879\text{ cm}^{-1}$  indicates C-H stretching vibrations caused by a weaker organic compound [46–49].

The prominent iron minerals hematite and magnetite were detected, with  $531$  and  $576\text{ cm}^{-1}$  spectra in the Pratima Garh sample. Their presence is possibly due to the replacement of  $\text{Fe}^{2+}$  and  $\text{Fe}^{3+}$  [50].

**Table 1.** FTIR spectra wave numbers with assigned mineralogy of the studied brick samples.

Assigned Mineralogy/ Assignment	Frequency with Relative Intensity ( $\text{cm}^{-1}$ )						Reference
	Sample No with Absorption Frequency and Relative Intensity ( $\text{cm}^{-1}$ )						
	Mouramora-1	Mouramora-2	Mouramora-3	Padumpukhuri	Pratima Garh	Rukmini Garh	
	1870VW	-	-	-	1876VW	1873W	
	-	-	-	-	-	1619VW	
Quartz	-	795S	795S	-	-	-	([15,28,51–53])
	778S	778S	778S	778S	776M	778SSp	
	693S	693M	694S	692M	693M	693S	
	460S	461S	-	-	463S	-	
	-	-	457S	458S	-	458S	
Microcline	-	-	-	-	1050S	-	([54])
Orthoclase	-	-	-	-	642W	-	([28])
Albite	-	-	-	-	725W	-	[16]
OH Stretching of Water Molecule	-	3851VW	-	-	3851VW	-	
	-	3746VW	-	-	3745W	-	
	-	3671VW	-	-	-	-	
OH stretching of inner hydroxyl group	-	-	-	-	-	3496WBr	[25,40,41,55]
	-	-	-	3475W	-	-	
Kaolinite	3468W	-	3460W	-	3462M	-	
	1080S	1080S	1081S	1084SBr	-	1081SBr	
Chlorite	-	3647VW	-	-	-	-	
Palygorskite	-	3565VW	-	-	-	-	[56]
Carbonate Minerals	1623W	1630W	1625W	1629W	1629W	-	[28]
	-	-	-	-	-	1788W	([28,42])
Magnetite	-	-	1384W	1381VW	-	-	
	-	-	-	-	576W	-	[57]



Table 1. Cont.

Assigned Mineralogy/Assignment	Frequency with Relative Intensity (cm <sup>-1</sup> )						Reference
	Sample No with Absorption Frequency and Relative Intensity (cm <sup>-1</sup> )						
	Mouramora-1	Mouramora-2	Mouramora-3	Padumpukhuri	Pratima Garh	Rukmini Garh	
Hematite	-	-	-	-	531W	-	[28,51]
	2922VW	2922VW	2919VW	2919VW	2919VW	2928VW	
Organic compound	2851VW	2851VW	2854VW	2854VW	2854VW	-	[27,28,57–59]
	-	-	-	-	2356VW	-	
	-	-	-	2004VW	-	-	
	1998VW	-	1998VW	-	-	1984VW	
	-	1878VW	1879VW	1879VW	-	-	

Abbreviations: VW—Very weak, W—Weak, M—Medium, S—Strong, Br—Broad, SBr—Strong and broad, SSP—Strong and sharp, WBr—Weak and broad.

### 3.2. Identification of Mineral through XRD Analysis

The XRD patterns of the studied brick samples are shown in Figure 5. Identified non-clay minerals include quartz, feldspars (orthoclase, microcline, oligoclase, sanidine, and albite), aragonite, dolomite, laumontite, ilmenite, siderite, hematite, chlorite, trona, pyrite, magnesite, wollastonite, goethite, and glauconite. Kaolinite was not present in the XRD results despite appearing in the FTIR results due to its amorphous nature. The minerals with the most intense reflections were quartz (3.34 Å), orthoclase (3.29 Å, 3.31 Å), and wollastonite (3.32 Å). Carbonate and iron-bearing minerals were noted.

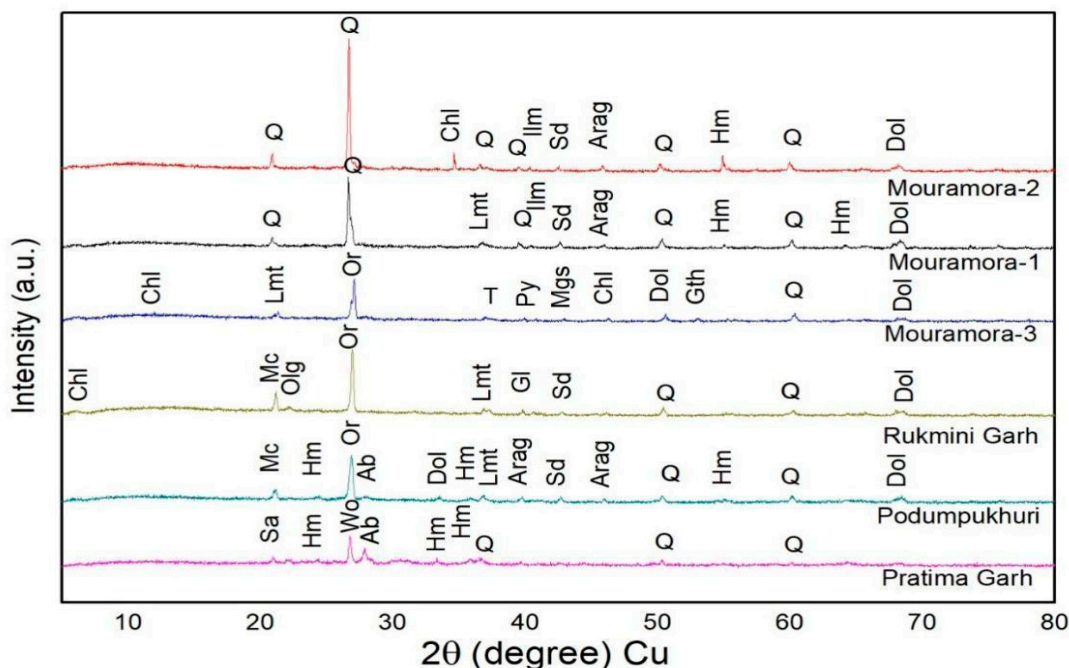


Figure 5. XRD pattern of studied brick samples (Q—Quartz, Feldspar (Or—Orthoclase, Mc—Microcline, Olg—Oligoclase, Sa—Sanidine, Ab—Albite), Arag—Aragonite, Dol—Dolomite, Lmt—Laumontite, Ilm—Ilmenite, Sd—Siderite, Wo—Wollastonite, Hm—Hematite, Chl—Chlorite, T—Trona, Py—Pyrite, Mgs—Magnesite, Gth—Goethite, and Gl—Glauconite).

### 3.3. The Firing Temperature Analysis Using FTIR and XRD

The IR spectra of dioctahedral and trioctahedral layer silicates display a very complex band system in the OH stretching region [40]. In the present study, the absorption bands at 3671–3851 cm<sup>-1</sup> and 3460–3496 cm<sup>-1</sup> were assigned to the OH stretching of water molecules and OH stretching of the inner hydroxyl group, respectively. However, upon heating the

samples, they underwent dehydration at 200 °C, continuing until 380 °C, resulting in the weakening of the 3400 cm<sup>-1</sup> broad band and the breaking of the crystal structure at 500 °C [40]. In addition, disorder in the octahedral and tetrahedral sheets is notable, with partial removal of the 535 cm<sup>-1</sup> Si-O bending band and broadening of the Si-O stretching bands in the 1100–1000 cm<sup>-1</sup> region [40]. This phenomenon implies a firing temperature of 500 °C. Additionally, at 500 °C, the absorption peak at 915 cm<sup>-1</sup> indicates that Al (OH) vibrations in the octahedral sheet structure begin to collapse [27,40,60,61]. The absence of 915 cm<sup>-1</sup> spectra in the studied samples suggests that all the samples were fired above 500 °C.

By increasing the temperature, the Si-O stretching band shifted toward higher frequencies and broadened, with the maximum intensity at around 1025 cm<sup>-1</sup> at 100 °C and shifting to 1036 cm<sup>-1</sup> at 600 °C [27,62]. The silicate structure disappeared when the clay was fired to 650 °C, and a broad symmetry band was detected at 1035 cm<sup>-1</sup> for red clay and 1080 cm<sup>-1</sup> for white clay [27,63]. The presence of an absorption band in five samples at around 1080–1084 cm<sup>-1</sup> indicates that white clay of kaolinitic composition was used in the investigated brick samples, which were fired at 650 °C.

The presence of hematite and magnetite, characterized by a peak at 540 cm<sup>-1</sup>, is an indication of iron oxides formed during fabrication firing processes above 650 °C [27,29,64]. However, the presence of hematite implies that they were fired in the open air or in a completely oxidizing atmosphere at the time of manufacture [65,66]. The presence of hematite and magnetite in the studied Pratima Garh sample confirms these manufacturing conditions, as well as the type of clay used, which is plausibly red clay. It can also be inferred that the artisans of Pratima Garh were well aware of the technology implemented in firing the bricks under both oxidizing and reducing atmosphere, which is inferred by the presence of peaks of 531 and 576 cm<sup>-1</sup>, respectively.

During the firing of clay, remarkable changes are noticed from 1000 to 1200 °C, where the X-ray diffractogram of quartz disappears. Quartz gradually decomposes from 800 to 1100 °C, peaking at 1100 °C and then disappearing. Up to 800 °C, all the decomposed phases contribute to the formation of a vitreous phase. At this point, the clay would be mostly amorphous, with some residual grains of quartz, neo-formed mullite, hematite, and other high-temperature mineral phases, like microcline. As a result, except for 1200 °C, quartz was a residual phase, i.e., a component of the raw clay that did not undergo chemical transformations during the firing stage. On the contrary, during the firing process, mullite, hematite, and other silicates were formed. At temperatures ranging from 700 to 900 °C, clays showed phyllosilicate destruction followed by vitrification, which was significant at temperatures above 1000 °C [67]. The presence of orthoclase, microcline, albite, hematite, and magnetite in the Pratima Garh, Rukmini Garh, Padumpukhuri, and Mouramora bricks supports the high firing temperature at more than 800 °C.

Clay deposits typically contain some organic material, but artisans can also add organic compounds to the ceramic paste during the preparation process to increase plasticity [68].

At 400–650 °C, depending on the type of flux and other raw materials used, the initial ingredients decompose, and CO<sub>2</sub>, S, and hydrocarbons are lost. Dehydration occurs at ~100 °C, followed by dehydroxylation of clay minerals at temperatures ranging from ~450 to 750 °C, depending on the type and purity of the clay [69]. Dehydration and dehydroxylation of relatively pure clay minerals occur at various temperatures depending on the clay minerals present. Chlorite loses water at a relatively high temperature, usually starting at ~750 °C, but this temperature is determined by the mineral chemistry. Illite (mica) transformation begins with dehydration at ~600–700 °C. When carbonate minerals are heated, they release carbon dioxide; for example, calcite decomposition begins at 650 °C. The temperature of phase transformation varies from sample to sample due to a variety of factors, such as mineral grain size, heating rate, and how easily the evolved carbon dioxide can be lost to the atmosphere [70]. At ~573 °C, alpha/low quartz structurally transforms into beta/high quartz. Because this transition involves rotation rather than bond breaking, the reaction is reversible, and any high-quality quartz that remains after the high-temperature soak will invert to low-quality quartz during the cooling phase of the

firing cycle. The brick expands as the temperature rises; however, if the cooling rate is too fast, highly damaging microcracking can occur [71].

The firing minerals that are generated during the production of pottery depend on a number of factors, including the composition of the clay, the materials added to it, the atmosphere, and the duration of the firing process. High-temperature minerals such as gehlenite and diopside are formed from the decomposition products of illite and calcite [10–12]. At 650 °C, calcite starts to break down; at 850 °C, high-temperature calc-silicates and aluminocalc-silicates, such as diopside and anorthite, are the products of this process. At temperatures higher than 830 °C, wollastonite—which is created when quartz and lime react from approximately 920 to 1000 °C—replaces gehlenite in systems that contain gehlenite [13]. The presence of wollastonite and feldspar (albite, orthoclase, and microcline) in the Pratima Garh, Padumpukhuri, Rukmini Garh, and Mouramora-3 brick samples indicates that the bricks were fired at temperatures above ~800 °C. The presence of the iron oxide minerals hematite and magnetite in the same sample, on the other hand, indicates that they were fired at temperatures higher than 650 °C, as indicated by the FTIR and XRD studies. In their analytical study of ancient pottery, the authors of [72] discovered that feldspars decompose at temperatures ranging from 900 to 950 °C. The presence of feldspars in the samples indicates that they were all fired at temperatures lower than 900 °C. This clearly shows that the Pratima Garh, Padumpukhuri, Rukmini Garh, and Mouramora-3 brick samples were fired at temperatures lower than 900 °C in oxidizing kiln atmospheric conditions. The estimated firing temperature of the samples is presented in Table 2. However, research concentrating on Thermogravimetry-Differential Thermal Analysis (TG-DTA), apparent porosity, water absorption, and other pertinent aspects are required to establish the accurate fire temperature of the investigated bricks.

**Table 2.** Estimation of firing temperature of studied brick samples based on FTIR and XRD analyses.

S.No.	Sample ID	Color	Type of the Clay	Estimation of Firing Temperature
1	Mouramora-1	Light red color	White clay	Below 650 °C
2	Mouramora-2	Light red color	White clay	Below 650 °C
3	Mouramora-3	Light red color	White clay	Above ~800 °C
4	Padum Pukhuri	Light red	White clay	Above ~800 °C
5	Rukmini Garh	Reddish yellow	White clay	Above ~800 °C
6	Pratima Garh	Weak red	Red clay	Above ~800 °C

### 3.4. The Firing Temperature Analysis Using SEM-EDS

SEM-EDS provides valuable information on the pore structure and the glassy phase development and is used to study systematically the internal morphology changes occurring when the materials are fired in a temperature range of 600 °C to 1300 °C; it can be employed and coupled with Energy Dispersive Spectrometer (EDS) for minerals detection [73]. Scanning Electron Microscope is a vital tool for examining ancient pottery and establishing ancient ceramic technology [74]. It has been found useful in many applications to characterize archaeological artifacts [75,76]. SEM with EDS analysis is non-destructive and capable of offering precise elemental composition information for the analysis of archaeological potsherds. The analysis evidences that the presence of Ca as fine-grained and evenly distributed calcite in clays significantly affects the development of vitrification if calcium present in the sample, say  $\text{CaCO}_3$ , dissociates into CaO and vitrification sets in around 850 °C.

The non-calcareous clays fired at temperatures below 800 °C produce no vitrification [77]. However, well-crystallized hematite is abundant in non-calcareous clays. The absence of vitrification in the studied bricks is evidence of a firing temperature below 800 °C during manufacturing by artisans, as well evidenced by FTIR and XRD studies. Firing at 900 °C produces much more pronounced changes in the clay body; sintering is quite advanced, and much vitrification has been produced [73]. Ref. [78] stated that continuous heating activates densification, which leads to a reduction in porosity, and it could lead to the generation of residual porosity and initial grain growth. They also opined



that this process initially creates necks between particles, followed by developments of cylindrical shape, interconnected pores, and lastly, pores change to a more spherical and isolated state as temperature increases. The SEM micrographs of the studied samples show the presence of such micropores (Figure 6a,b), as well as change in pores shape to spherical and isolated state (Figure 6c–f), suggesting that the heating temperature increased in the bricks of Mouramora-3, Padum Pukhuri, Pratima Garh, and Rukmini Garh compared with the Mouramora-1 and Mouramora-2 bricks.

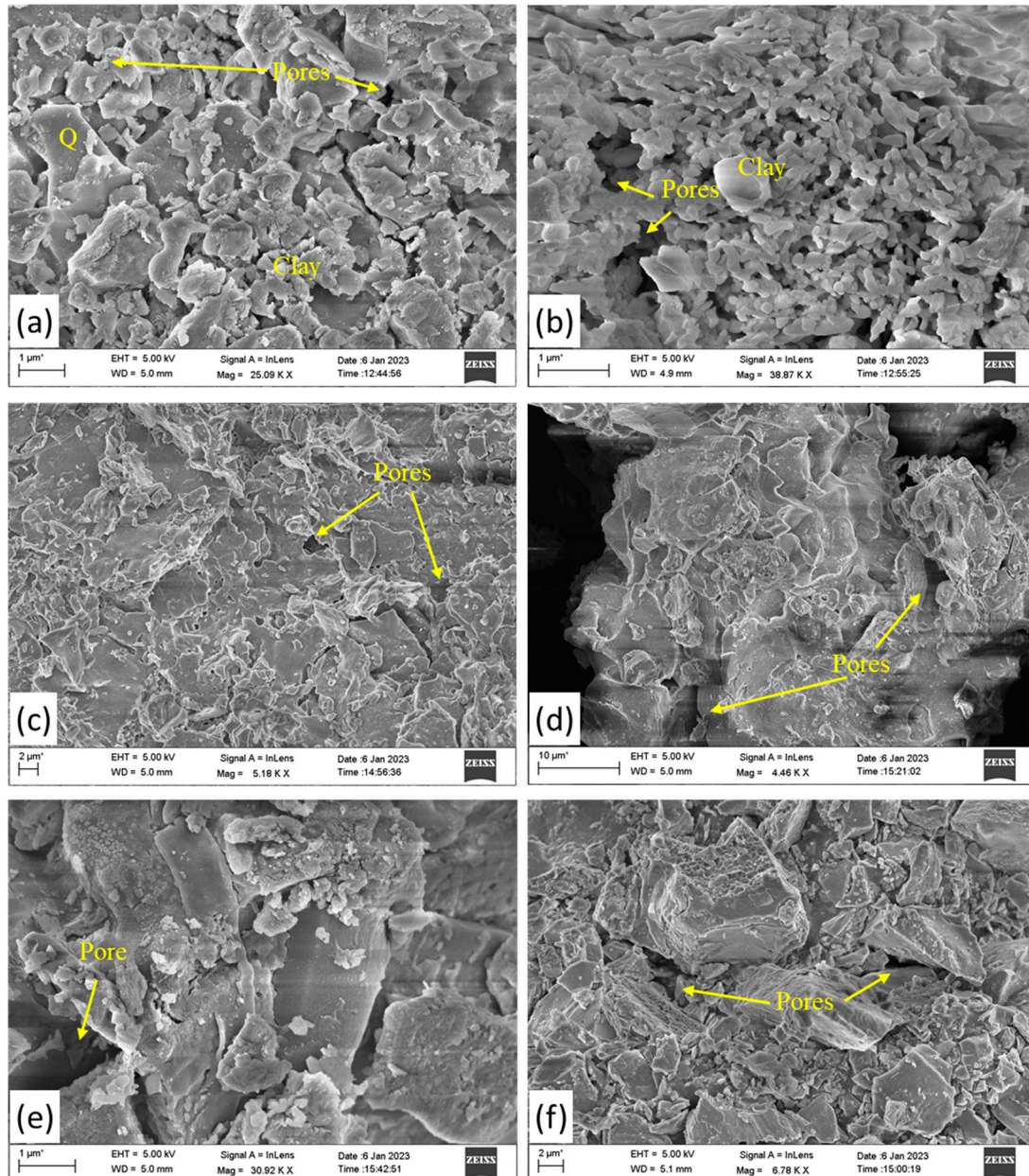


**Figure 6.** Representative SEM backscattered image of surface morphology of studied fired brick samples. (a) Mouramora-1, (b) Mouramora-2, (c) Mouramora-3, (d) PadumPukhuri, (e) Pratima Garh, (f) Rukmini Garh.

The chemical composition of the samples was obtained using EDS analysis, and their representative spectra are shown in Figure 7. From the EDS analysis, the potsherds mainly have high concentrations of silica ( $\text{SiO}_2$ ), alumina ( $\text{Al}_2\text{O}_3$ ), and fluxes ( $\text{Na}_2\text{O}$ ,  $\text{K}_2\text{O}$ ,  $\text{Fe}_2\text{O}_3$ ,  $\text{CaO}$ ,  $\text{MgO}$  and  $\text{TiO}_2$ ), as they were identified in all the samples except for  $\text{Na}_2\text{O}$ ,  $\text{CaO}$ ,

and  $\text{TiO}_2$  in Padum Pukhuri,  $\text{CaO}$  and  $\text{TiO}_2$  in Mouramora 1, and  $\text{CaO}$  in Mouramora 2. Researchers claim that the total flux concentration within potsherds provides valuable insights into the thermal behavior of bricks, contributing to the formation of a vitreous or glassy phase [79,80]. When multiple components like  $\text{Na}_2\text{O}$ ,  $\text{TiO}_2$ ,  $\text{Fe}_2\text{O}_3$ ,  $\text{CaO}$ , and  $\text{MgO}$  are present along with  $\text{SiO}_2$  and  $\text{Al}_2\text{O}_3$ , a large portion of the liquid is generated, which is referred to as a glassy or vitreous phase [81]. The total flux content of potsherds was determined using the formula  $\text{Total Flux Content} = \text{RO} + \text{R}_2\text{O} + \text{Fe}_2\text{O}_3 + \text{TiO}_2$ , where  $\text{RO} = \text{CaO} + \text{MgO}$  and  $\text{R}_2\text{O} = \text{K}_2\text{O} + \text{Na}_2\text{O}$  [81,82]. In the present study, the total flux content was calculated, with values ranging from 8.91 to 25.77 wt.%, with samples from Mouramora-3, Padum Pukhuri, Pratima Garh, and Rukmini Garh showing higher values, whereas Mouramora-1 and Mouramora-2 bricks showed lower values.

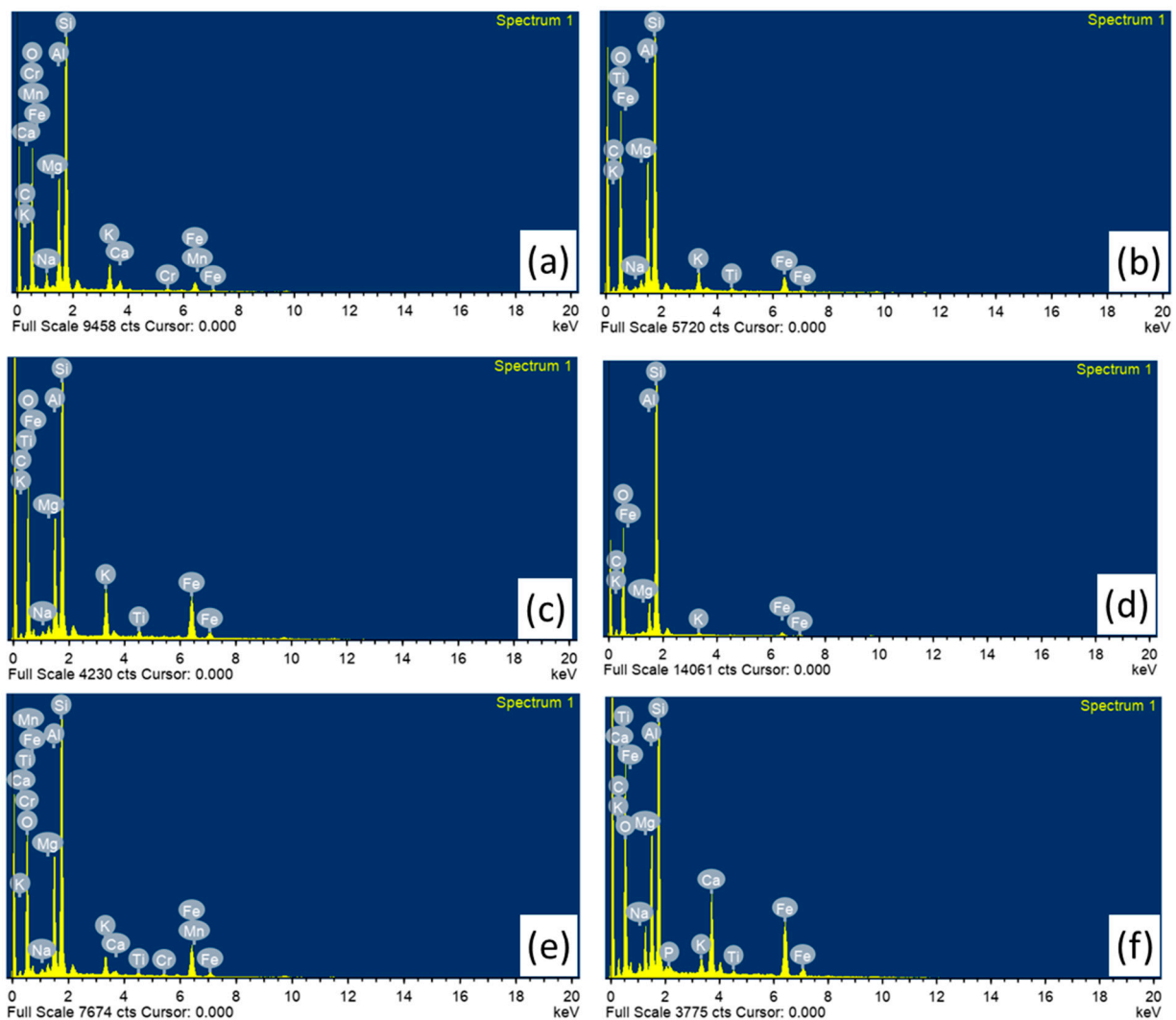


**Figure 7.** Representative EDS pattern of studied fired brick samples: (a–c) Mouramora-1, Mouramora-2, and Mouramora-3, respectively; (d) PadumPukhuri; (e) Rukmini Garh; and (f) Pratima Garh.

If the flux concentration ( $\text{K}_2\text{O}$ ,  $\text{Fe}_2\text{O}_3$ ,  $\text{CaO}$ ,  $\text{MgO}$ , and  $\text{TiO}_2$ ) is more than 9%, the clays are classified as low refractory, and they are classified as high refractory if the fluxes in the sample are less than 9% [29]. On the other hand, the clays containing  $\text{CaO}$  greater than 6% are known as calcareous clays, and those containing  $\text{CaO}$  less than 6% are known as non-calcareous clays [63]. Based on the above statement and EDS results, it is inferred that all the baring Pratima Garh bricks were made from non-calcareous clay. Moreover, Mouramora-1, Mouramora-2, and Padum Pukhuri showed high refractory clay characteristics, and Mouramora-3, Pratima Garh, and Rukmini Garh reflected low refractory characteristics.

From the analysis, silica was the major element in all the bricks, with a percentage that varied from 66.81% to 82.10%. All the bricks with low refractory clay contained high iron oxide concentrations, ranging from 10.88% to 12.84%. The chromium concentrations were noticed in two of the studied samples: Mouramora-1 (0.53%) and Rukmini Garh (0.47%). It should be noted, however, that the pottery composition depends both on the clay source and the recipe used to prepare the clay paste [12]. The variation of the chemical composition in bricks may imply that the pottery comes from different production sites or reflects the natural inhomogeneity of local clay deposits and the application of different manufacturing processes in local workshops. The SEM-EDS results for the firing temperature analysis are in good agreement with the FT-IR and XRD results.

### 3.5. TL, OSL, and IRSL Results

TL, OSL, and IRSL equivalent doses (E.D.) were evaluated for all samples; because no mineralogical phase separation was performed on the brick samples, any luminescent mineral contributes to the emission, quartz and feldspars being the main emitters. Both quartz and feldspars have a TL emission in the blue region of the spectrum, and their contribution is not separate. For what concerns OSL, while blue light stimulates the emission of both quartz and feldspars, IR light only stimulates feldspars; for this very reason, both OSL and IRSL were performed. Typical examples of TL glow curves are shown in Figure 8a. Based on the plateau test, which allows us to identify the thermally stable portion of the curves (Aitken, 1985), the TL signals were integrated between 300 and 350 °C. Plotting the intensity of the TL signal vs. the laboratory-imparted dose, E.D. was extrapolated by linear regression, as illustrated in Figure 8b. The results of such evaluations are summarized in Table 3.

Typical OSL/IRSL shine-down curves are shown in Figure 8c–e. The samples were stimulated for 40 s in case of OSL measurement and 100 s for IRSL. The preheat temperature was 200 °C for 10 s while the cut-heat was 180 °C, and it was chosen using a preheat plateau test. For the E.D. determination, the initial part of the OSL/IRSL decay curve was used, specifically the first 0.6 s for OSL and the first 1.6 s for IRSL. The background was assumed as the average signal of the last 10 s (OSL) or 20 s (IRSL) of stimulation. Plotting the intensity of the OSL/IRSL signal vs. the laboratory-imparted dose, E.D. was determined through the interpolation of the natural signal on the linear regression, as illustrated in Figure 8d,f.

In general, it can be said that the luminescence signals of the samples are rather weak, especially as regards the OSL signal. For this reason, it was possible to use this technique only to date the Padum Pukhuri sample, whose OSL curves have a sufficiently high intensity. IRSL, on the other hand, is the technique that gave the most intense signals for all samples.

By looking at the dating results obtained with TL, OSL, and IRSL (Table 3), it is possible to observe that the low luminescence intensity of the samples caused high errors in the ages obtained. The results obtained with TL are in good agreement with those obtained with IRSL, except for the Padum Pukhuri sample. For the latter sample there is instead a good agreement between the ages obtained with TL and OSL.

It is well-known that minerals like feldspars can provide underestimated ages for the presence of anomalous fading [83], a malign phenomenon due to the loss of charge from thermally stable defect sites via non-thermal mechanisms. A specific fading test was, therefore, performed at room temperature for one month, and a significant loss of signal was observed, as shown in Figure 9 for the Padum Pukhuri sample. Therefore, fading evaluations were performed on all samples for all the luminescence techniques used (TL, IRSL, and OSL). For each sample and for each type of luminescence, the *g*-values [84] were determined (see Table 4). The ages of the samples obtained were then recalculated according to the equation reported in [84] to obtain the dates corrected for the fading phenomenon (Table 4).



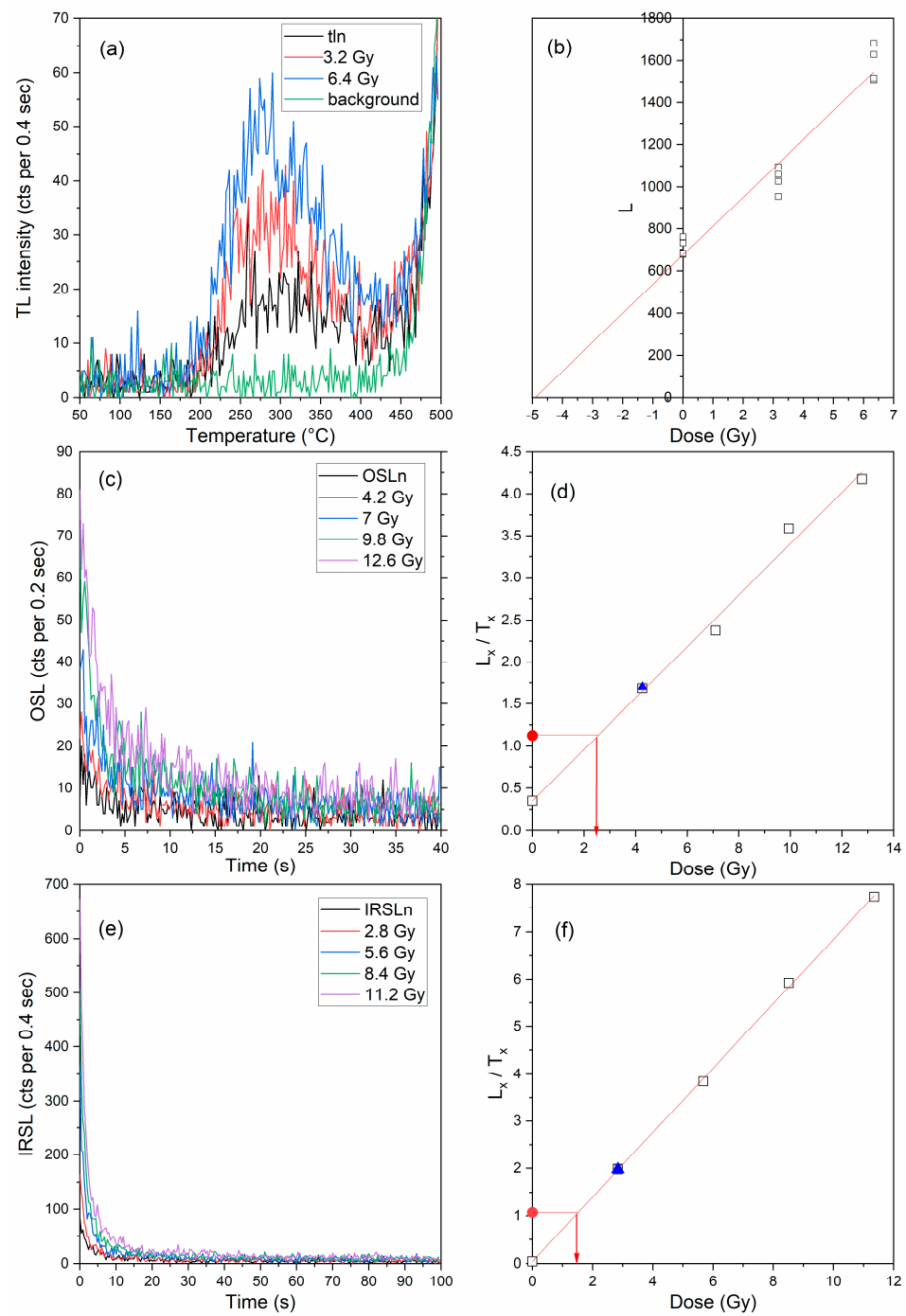


**Figure 8.** (a) TL glow curves, (c) OSL, and (e) IRSL shine-down curves of the Padum Pukhuri sample. (b) Growth curve of the TL signal with imparted additive dose. TL glow curves were integrated between 300 and 3500 °C, and the signal of the background in the same temperature interval (green line) was subtracted. Sensitivity-corrected (d) OSL and (f) IRSL response to a fixed dose vs. the laboratory-imparted regenerative dose. The red dot is the natural signal, and the blue triangle is the recycling ratio point.

**Table 3.** Saturation water contents (W), a-values, and U, Th, and K<sub>2</sub>O concentrations, E.D., dose rates for quartz and feldspars, ages, dates, and errors obtained with different luminescence techniques on brick samples.

SAMPLE ID	W (%)	a Value	ppm U (±5%)	ppm Th (±5%)	K <sub>2</sub> O (±3%)	E.D. (Gy)	Dose Rate (mGy/a)	Age (y)	Date	Error
Mour1 TL	18	0.14	4.1	12.9	2.98	2.2 ± 0.3	6.9 ± 0.3	320	1700	60
Mour-1 IRSL	18	0.14	4.1	12.9	2.98	2.6 ± 0.8	7.5 ± 0.3	350	1670	90
Mour-2 TL	23	0.18	4.3	13.8	2.56	2.7 ± 0.3	7.2 ± 0.4	380	1640	60
Mour-2 IRSL	23	0.18	4.3	13.8	2.56	3.1 ± 0.5	7.8 ± 0.4	400	1620	90
Mour-3 TL	24	0.14	4.2	13.4	3.52	2.7 ± 0.3	7.6 ± 0.4	360	1640	70
Mour-3 IRSL	24	0.14	4.2	13.4	3.52	1.8 ± 0.2	7.7 ± 0.4	230	1790	60
Prat TL	33	0.14	5.0	15.8	3.52	3.6 ± 0.3	7.3 ± 0.4	490	1530	60
Prat IRSL	33	0.14	5.0	15.8	3.52	4.2 ± 0.3	7.9 ± 0.4	530	1490	70
PadumTL	30	0.25	2.7	8.5	1.48	4.9 ± 0.4	4.9 ± 0.2	1000	1020	120
PadumOSL	30	0.25	2.7	8.5	1.48	4.2 ± 1.0	4.9 ± 0.2	860	1160	250
PadumIRSL	30	0.25	2.7	8.5	1.48	1.6 ± 0.2	5.5 ± 0.2	290	1730	60

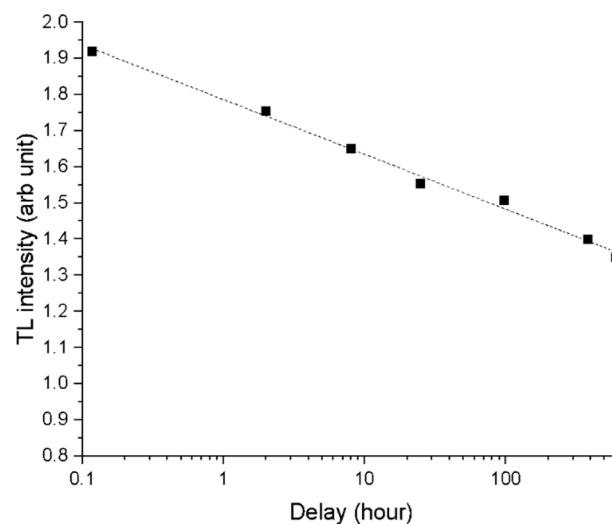


**Figure 9.** Anomalous fading TL data obtained from the Padumpukhuri sample. Seven samples were irradiated with a dose of 6.4 Gy. A sample was measured immediately after irradiation, while the others were kept in the dark for periods ranging from one hour to a month.

**Table 4.** g-values, ages, and dates corrected for anomalous fading.

SAMPLE ID	g-Value	Age Faded	Date Faded
Mour-1 (TL)	6.8 ± 0.4	630 ± 130	1390 ± 130
Mour-1 (IRSL)	7.9 ± 0.5	920 ± 220	1100 ± 220
Mour-2 (TL)	8.4 ± 1.8	1010 ± 300	1010 ± 270
Mour-2 (IRSL)	5.7 ± 1.5	870 ± 250	1150 ± 250
Mour-3 (TL)	9.0 ± 0.3	1170 ± 280	850 ± 280
Mour-3 (IRSL)	9.8 ± 0.3	910 ± 250	1110 ± 250
Prat (TL)	8.6 ± 2.1	1410 ± 390	610 ± 390
Prat (IRSL)	9.0 ± 0.2	1860 ± 300	160 ± 500
Padum (TL)	3.4 ± 0.7	1350 ± 180	670 ± 180
Padum (OSL)	3.3 ± 0.6	1140 ± 360	880 ± 360
Padum (IRSL)	9.1 ± 0.1	1040 ± 200	980 ± 200

The high g-values (>7%) obtained for nearly all the samples suggest the presence of some luminescent mineralogical phase other than feldspars with a high fading rate. In the literature, Garcia Guinea et al. [85] reported a TL emission of kaolinite in the blue region of

the spectrum. Ten years later, it was found that this mineral could potentially be valid for dosimetric purposes since it is sensitive to radiation and possesses a good dose linearity in the range of 50 mGy to 8 Gy [86]. However, the stability of the TL signal during six months of storage shows an initial rapid decay (ca. 60%) followed by a mild slope reaching stability after six months. Moreover, this mineral stands as a very promising candidate for IRSL dating based on the very good IRSL response of this material to artificial beta irradiation [87].

Based on these results and on data obtained using FTIR and XRD analyses that confirm the presence of kaolinite in all the bricks studied, the dosimetric properties of kaolinite were more deeply investigated. Hence, the TL, OSL, and IRSL measurements were carried out on kaolinite coming from Monte Bracco (Barge, CN, Italy). The sample presented luminescence signals either when heated or when illuminated with blue and IR light; Figure 10 shows TL, OSL and IRSL signals when irradiated with a dose from 9 to 92 Gy. There was a linear growth of signal with dose in TL (at least up to 92 Gy), OSL, and IRSL (up to about 37 Gy). At this point, the stability of the TL, OSL, and IRSL signals of kaolinite were investigated. A fading test was performed, and it was noted that the measured luminescence signal (TL, OSL, and IRSL) decreases as the time between irradiation and measurement increases (Figure 11). Unfortunately, it was not possible to determine the *g*-value for any of the luminescence techniques used as the decay of the luminescence signals does not follow the exponential decay law used for feldspars. The significant loss of luminescent signal over time, however, allows us to identify kaolinite as a possible cause of the high *g*-values obtained on the bricks analyzed in this work.

### 3.6. Chronology of Bricks

The mineralogical characterization and chronology in the present study infer the existence of two distinct groups, with pottery technology having different firing temperatures. One, characterized by a firing temperature below 650 °C, resembles pottery from the XI-XIV centuries CE on the South Bank of the River Brahmaputra, and the other, characterized by a firing temperature above 650 °C up to 830 °C, resembles pottery from the VII-X centuries CE (Table 5) on the North Bank of the River Brahmaputra. These two divisions could indicate two different civilizations with technologies that allowed them to fire the bricks in different oxidizing kiln atmospheric conditions. From the present investigation, it can be summarized that the first group of people lived during the VII-X centuries CE, were technologically enhanced, and their state boundaries might be limited to the Northern bank of Brahmaputra, as well as the foothills of Arunachal Pradesh (studied bricks were from Padum Pukhuri, Pratima Garh, and Rukmini Garh). The second group of people, who lived during the XI-XIV centuries CE, were technologically less enhanced than the first group, and their state boundaries might be confined to the Southern bank of the river Brahmaputra. Sheikh [88] dated bricks from the Kamakhya Temple of Assam, India, suggesting two distinct age ranges peaked at 500 CE and 800 CE. He opined that some segments of the existing Kamakhya temple might have been reconstructed later in 800 CE, when brick production technology was more advanced than that of one of the earlier inhabitants. Hence, it can be assumed that the bricks found in the Northern bank of Brahmaputra, as well as the foothills of Arunachal Pradesh (Padum Pukhuri, Pratima Garh, and Rukmini Garh), along with those bricks from Kamakhya Temple dating to 800 CE, were probably manufactured by a similar group of people residing in that time.



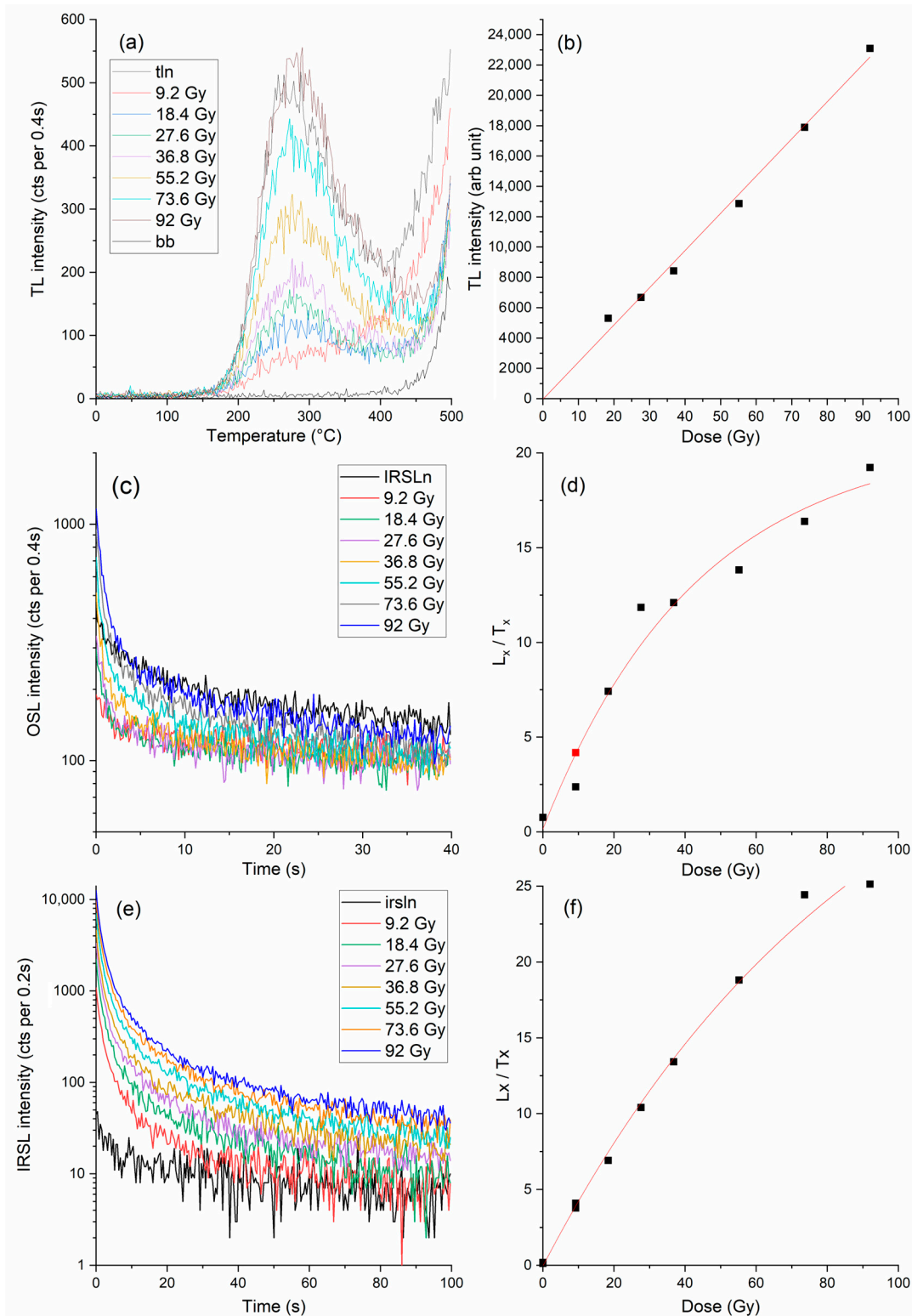


**Figure 10.** Luminescence signals of kaolinite. (a) TL glow curves and (b) corresponding growth of TL signal with dose; (c) OSL shine-down curves and (d) corresponding growth of OSL signal with dose; and (e) IRSL shine-down curves and (f) corresponding growth of IRSL signal with dose.

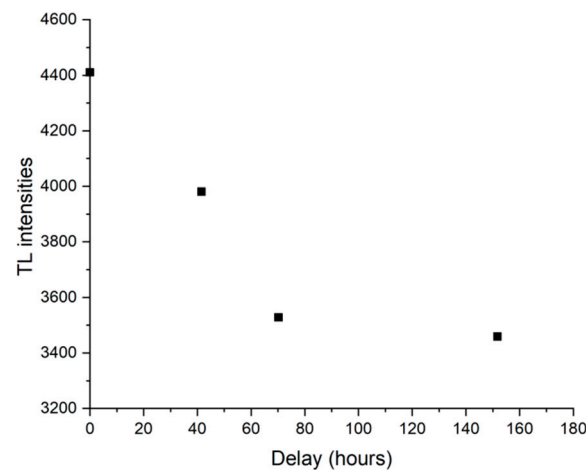


**Figure 11.** Anomalous fading TL data obtained from kaolinite. The sample was irradiated with 92 Gy, and the TL signal was measured. A test dose equal to 10 Gy was then imparted on the same aliquot and used to normalize the signal in order to consider the sensitization of the sample between the different irradiation and measurement cycles. At this point, the same aliquot was irradiated again with 792 Gy and stored in the dark for a certain time, after which the TL curve and the related test dose were recorded.

**Table 5.** Estimated ages, firing temperature, and type of clay used in the studied archaeological sites.

Name of Archaeological Sites	Type of Clay Used	Calculated Age	Estimated Firing Temperature
Mouramora-1	Non-calcareous		Below 650 °C
Mouramora-2	Non-calcareous	XI-XIV sec CE	Below 650 °C
Mouramora-3	Non-calcareous		Above ~800 °C
Pratima Garh	Calcareous	VII-X sec CE (i.e.,	Above ~800 °C
Padum Pukhuri	Non-calcareous	pre-Ahom)	Above ~800 °C
Rukmini Garh	Non-calcareous	Not datable	Above ~800 °C

It is relevant to remember that dating the bulk material of construction bricks can mislead from the correct age since the dated event corresponds to the last heating (>500 °C) of the material, generally related to brick production, which can be significantly different from that of the construction, also due to the practice of reusing old bricks. However, it is noteworthy that the cause of technological changes between the two groups might be a scope for future research.

The use of production materials like calcareous and non-calcareous clay having low and high refractory nature for making bricks also infers that the bricks might be produced in different production sites or reflect the natural inhomogeneity of local clay deposits and the application of different manufacture processes in local workshops.

#### 4. Conclusions

The comprehensive application of various spectroscopic techniques, including Fourier Transform Infrared Spectroscopy (FTIR), X-ray Diffraction (XRD), and Scanning Electron Microscopy with Energy Dispersive X-ray Spectroscopy (SEM-EDS), alongside absolute dating methodologies such as Thermoluminescence (TL), Optically Stimulated Luminescence (OSL), and Infrared Stimulated Luminescence (IRSL), yielded significant insights into the chronology and technological practices at the archaeological site under study.

The data reveal the existence of two distinct stratified groups of inhabitants, each characterized by unique brick production methods that reflect their technological capabilities and environmental adaptations. The first group, dating back approximately 700 to 1000 years ago, showed a more advanced mastery of firing techniques, achieving temperatures exceeding 800 °C. This is evidenced by the analysis of the Pratima Garh and

Padum Pukhuri samples, which show the high-temperature conditions under which their bricks were produced. This suggests that these earlier inhabitants possessed a sophisticated understanding of kiln construction and thermal control, likely contributing to the durability and quality of their brick materials.

In contrast, the second group of inhabitants, who occupied the site between 1100 and 1400 years ago, employed less advanced firing techniques. Analysis of Mouramora samples from this period indicates that their bricks were fired at temperatures below 650 °C. This difference in firing temperature not only points to a divergence in technological knowledge but may also reflect variations in socio-economic conditions, resource availability, and cultural practices between the two groups.

Overall, the integrated use of these advanced analytical methods provided a nuanced understanding of the technological evolution at this archaeological site. The findings underscore the complexity of cultural and technological development over time, highlighting how different communities adapted their techniques to suit their specific environmental and social contexts. This multidisciplinary approach offers a comprehensive framework for interpreting the material culture and technological progress of past societies, shedding light on the dynamic interplay between human innovation and environmental constraints.

**Author Contributions:** Conceptualization, R.R.S., C.D.T. and N.A.; methodology, R.R.S. and C.D.T.; software, S.K. and C.D.T.; validation, C.D.T., A.G. and L.P.; formal analysis, C.D.T., A.G. and L.P.; investigation, R.R.S., N.A., C.D.T., S.K., A.G. and L.P.; resources, R.R.S.; data curation, R.R.S. and C.D.T.; writing—original draft preparation, C.D.T. and R.R.S.; writing—review and editing, R.R.S., N.A., C.D.T., S.K., A.G. and L.P.; visualization, R.R.S.; project administration, R.R.S.; funding acquisition, R.R.S., N.A. and S.K. All authors have read and agreed to the published version of the manuscript.

**Funding:** This research was funded by Indian National Science Academy (INSA) grant number HS/RC/300.

**Institutional Review Board Statement:** Not applicable.

**Informed Consent Statement:** Not applicable.

**Data Availability Statement:** The original contributions presented in the study are incorporated in the article, further inquiries can be directed to the corresponding author or first author.

**Acknowledgments:** At the very outset, we extend our sincere gratitude to the Indian National Science Academy (INSA) for providing us with financial assistance to conduct the project (Sanction No: HS/RC/300). We also gratefully acknowledge the Directorate of Archaeology, Government of Assam, India, for providing us the permission to collect samples from Archaeological sites. Further, we are deeply thankful to the CSIR-North East Institute of Science & Technology, Jorhat, India, for providing the necessary facilities for the SEM-EDS, XRD and FTIR analysis of the studied brick samples. We also gratefully acknowledge the anonymous reviewers and handling editor for their constructive and helpful comments, which helped us to polish the manuscript in this present form.

**Conflicts of Interest:** The authors declare no conflicts of interest.

## References

1. Weaver, M.E. *Conserving Buildings: Guide to Techniques and Materials, Revised Edition*; John Wiley & Sons, Inc.: Hoboken, NJ, USA, 1997; Available online: <https://www.biblio.com/book/conserving-buildings-guide-techniques-materials-revised/d/1573100919> (accessed on 30 March 2024).
2. Fernandes, F.M.; Lourenço, P.B.; Castro, F. Ancient Clay Bricks: Manufacture and Properties. In *Materials, Technologies and Practice in Historic Heritage Structures*; Dan, M.B., Příkryl, R., Török, Á., Eds.; Springer: Dordrecht, The Netherlands, 2010; pp. 29–48. [CrossRef]
3. Johari, I.; Said, S.; Hisham, B.; Bakar, A.; Ahmad, Z.A. Effect of the change of firing temperature on microstructure and physical properties of clay bricks from Beruas (Malaysia). *Sci. Sinter.* **2010**, *42*, 245–254. [CrossRef]
4. Mostaghelchi, M.; Zahiri, R.; Miremadi, S.H.; Ebadi, A.G. Use of Mica Mineral Powder in Bricks Industry to Improve the Performances. *Asian J. Chem.* **2013**, *25*, 9144–9148. [CrossRef]
5. Rasmussen, K.L.; De La Fuente, G.A.; Bond, A.D.; Mathiesen, K.K.; Vera, S.D. Pottery firing temperatures: A new method for determining the firing temperature of ceramics and burnt clay. *J. Archaeol. Sci.* **2012**, *39*, 1705–1716. [CrossRef]
6. Amkpa, J.A.; Badaruzaman, N.A.; Aramjat, A.B. Influence of Sintering Temperatures on Physico-Mechanical Properties and Microstructure of Refractory Fireclay Bricks. *Int. J. Eng. Technol.* **2016**, *8*, 2588–2593. [CrossRef]

7. Amkpa, J.A.; Badarulzaman, N.A.; Aramjat, A.B. Impact of Sintering Temperatures on Microstructure, Porosity and Mechanical Strength of Refractory Brick. *Mater. Sci. Forum* **2017**, *888*, 66–70. [CrossRef]
8. Karaman, S.; Erşahin, S.; Günal, H. Firing temperature and firing time influence on mechanical and physical properties of clay bricks. *J. Sci. Ind. Res.* 2006. Available online: <https://www.semanticscholar.org/paper/Firing-temperature-and-firing-time-influence-on-and-Karaman-Er%C5%9Fahin/f0cf8fe0caf2127e9b95492b85981a3292925d16> (accessed on 2 April 2024).
9. Velraj, G.; Janaki, K.; Musthafa, A.M.; Palanivel, R. Estimation of firing temperature of some archaeological pottery shreds excavated recently in Tamilnadu, India. *Spectrochim. Acta Part A Mol. Biomol. Spectrosc.* **2009**, *72*, 730–733. [CrossRef]
10. Maritan, L.; Nodari, L.; Mazzoli, C.; Milano, A.; Russo, U. Influence of firing conditions on ceramic products: Experimental study on clay rich in organic matter. *Appl. Clay Sci.* **2006**, *31*, 1–15. [CrossRef]
11. İssi, A.; Kara, A.; Alp, A.O. An investigation of Hellenistic period pottery production technology from Harabebezikan/Turkey. *Ceram. Int.* **2011**, *37*, 2575–2582. [CrossRef]
12. Papachristodoulou, C.; Oikonomou, A.; Ioannides, K.; Gravani, K. A study of ancient pottery by means of X-ray fluorescence spectroscopy, multivariate statistics and mineralogical analysis. *Anal. Chim. Acta* **2006**, *573–574*, 347–353. [CrossRef]
13. Böhme, N.; Hauke, K.; Neuroth, M.; Geisler, T. In situ Raman imaging of high-temperature solid-state reactions in the CaSO<sub>4</sub>–SiO<sub>2</sub> system. *Int. J. Coal Sci. Technol.* **2019**, *6*, 247–259. [CrossRef]
14. Ghale, D.B.; Bohara, N.B.; Duwal, N.; Bhattarai, J. Investigation on the mineralogical phase of ancient brick samples of Kathmandu Valley (Nepal) using XRD and FTIR analysis. *Rasayan J. Chem.* **2019**, *12*, 402–408. [CrossRef]
15. Keller, W.D.; Pickett, E.E. Absorption of infrared radiation by powdered silica minerals. *Am. Mineral.* **1949**, *34*, 855–868.
16. Legodi, M.A.; De Waal, D. Raman spectroscopic study of ancient South African domestic clay pottery. *Spectrochim. Acta Part A Mol. Biomol. Spectrosc.* **2007**, *66*, 135–142. [CrossRef] [PubMed]
17. Mendelovici, E. Comparative study of the effects of thermal and mechanical treatments on the structures of clay minerals. *J. Therm. Anal.* **1997**, *49*, 1385–1397. [CrossRef]
18. Rutherford, J.S.; Almond, M.J.; Nunn, P.D. Analysis of pottery samples from Bourewa, the earliest known Lapita site in Fiji. *Spectrochim. Acta Part A Mol. Biomol. Spectrosc.* **2012**, *85*, 155–159. [CrossRef]
19. Velraj, G.; Seetha, D.; Hemamalini, R. FT-IR, XRD, Porosity and TG-DTA Analysis of Archaeological Potteries Excavated from Kottapuram, Kerala, South India. *Elixir Vib. Spec.* **2014**, *66*, 20815–20819.
20. Aitken, M.J. *Thermoluminescence Dating*; Academic Press Inc.: London, UK, 1985.
21. Aitken, M.J. *An Introduction to Optical Dating: The Dating of Quaternary Sediments by the Use of Photon-Stimulated Luminescence*; Oxford Science Publications: Oxford, UK, 1998.
22. Galli, A.; Martini, M.; Montanari, C.; Panzeri, L.; Sibilila, E. TL of fine-grain samples from quartz-rich archaeological ceramics: Dosimetry using the 110 and TL peaks. *Radiat. Meas.* **2006**, *41*, 1009–1014. [CrossRef]
23. Galli, A.; Sibilila, E.; Martini, M. Ceramic chronology by luminescence dating: How and when it is possible to date ceramic artefacts. *Archaeol. Anthropol. Sci.* **2020**, *12*, 190. [CrossRef]
24. Dhanapandian, S.; Shanthi, M.; Manoharan, C. FTIR and Mossbauer Studies on Industrial Clay Bricks from Three Different Regions of Tamilnadu State. *Int. J. Curr. Res.* **2010**, *4*, 122–126.
25. Govindasamy, A.; Viruthagiri, G.; Ramesh, K. FI-IR Spectroscopic and Porosity Studies to Estimate the Firing Temperature of the Clay Brick. *Intern. J. Appl. Eng. Res.* **2019**, *14*, 2904–2909.
26. Kiruba, S.; Ganesan, S. FT-IR and Micro-Raman spectroscopic studies of archaeological potteries recently excavated in Poompuhar, Tamilnadu, India. *Spectrochim. Acta Part A Mol. Biomol. Spectrosc.* **2015**, *145*, 594–597. [CrossRef]
27. Raja Annamalai, G.; Ravisankar, R.; Rajalakshmi, A.; Chandrasekaran, A.; Rajan, K. Spectroscopic characterization of recently excavated archaeological potsherds from Tamilnadu, India with multi-analytical approach. *Spectrochim. Acta Part A Mol. Biomol. Spectrosc.* **2014**, *133*, 112–118. [CrossRef] [PubMed]
28. Ramasamy, V.; Rajkumar, P.; Ponnusamy, V. Depth wise analysis of recently excavated Vellar river sediments through FTIR and XRD studies. *Indian J. Phys.* **2009**, *83*, 1295–1308. [CrossRef]
29. Ravisankar, R.; Raja Annamalai, G.; Naseerutheen, A.; Chandrasekaran, A.; Prasad, M.V.R.; Satpathy, K.K.; Maheswaran, C. Analytical characterization of recently excavated megalithic sarcophagi potsherds in Veeranam village, Tiruvannamalai dist., Tamilnadu, India. *Spectrochim. Acta Part A Mol. Biomol. Spectrosc.* **2013**, *115*, 845–853. [CrossRef] [PubMed]
30. Ravisankar, R.; Naseerutheen, A.; Rajalakshmi, A.; Raja Annamalai, G.; Chandrasekaran, A. Application of thermogravimetry–differential thermal analysis (TG–DTA) technique to study the ancient potteries from Vellore dist, Tamilnadu, India. *Spectrochim. Acta Part A Mol. Biomol. Spectrosc.* **2014**, *129*, 201–208. [CrossRef] [PubMed]
31. Velraj, G.; Sathya, P.; Champion, P.M.; Ziegler, L.D. *Mineralogical Appraisal Of Ancient Brick Samples Using FT-IR Spectroscopy*; American Institute of Physics: College Park, MD, USA, 2010; pp. 307–308. [CrossRef]
32. Sheikh, M.R.; Barua, A.G. X-ray Diffraction and Fourier Transform Infrared Spectra of the Bricks of the Kamakhya Temple. *Indian J. Pure Appl. Phys.* **2013**, *15*, 745–748.
33. Chen, P.-Y. Table of Key Lines in X-ray Powder Diffraction Patterns of Minerals in Clays and Associated Rocks. 1977. Available online: <https://scholarworks.iu.edu/dspace/items/61872b58-e6ab-4827-8b49-4b8ce8f754b4>, (accessed on 11 June 2024).
34. Lindholm, R.C. *A Practical Approach to Sedimentology*; Springer: Dordrecht, The Netherlands, 1987. [CrossRef]



35. Tucker, M. *Techniques in Sedimentology*; Blackwell Scientific Publications: Oxford, London, Edinburgh, Boston, Melbourne, 1988; Available online: <https://www.semanticscholar.org/paper/Techniques-in-sedimentology-Tucker/8f7d146ef7f60092851570958bf1d81525820305> (accessed on 11 June 2024).
36. Zimmerman, D.W. Thermoluminescence dating using fine grains from pottery. *Archaeometry* **1971**, *13*, 29–52. [[CrossRef](#)]
37. Murray, A.S.; Roberts, R.G. Measurement of the equivalent dose in quartz using a regenerative-dose single-aliquot protocol. *Radiat. Meas.* **1998**, *29*, 503–515. [[CrossRef](#)]
38. Prescott, J.R.; Hutton, J.T. Cosmic ray contributions to dose rates for luminescence and ESR dating: Large depths and long-term time variations. *Radiat. Meas.* **1994**, *23*, 497–500. [[CrossRef](#)]
39. Panzeri, L.; Galli, A.; Maspero, F.; Saleh, M.; Martini, M. The activities of the LAMBDA (Laboratory of Milano Bicocca university for Dating and Archaeometry): What's new? *J. Phys. Conf. Ser.* **2022**, *2204*, 012047. [[CrossRef](#)]
40. Elsass, F.; Olivier, D. Infra-red and electron spin resonance studies of clays representative of the sedimentary evolution of the basin of Autun. *Clay Min.* **1978**, *13*, 299–308. [[CrossRef](#)]
41. Bukalo, N.N.; Ekosse, G.-I.E.; Odiyo, J.O.; Ogola, J.S. Fourier Transform Infrared Spectroscopy of Clay Size Fraction of Cretaceous-Tertiary Kaolins in the Douala Sub-Basin, Cameroon. *Open Geosci.* **2017**, *9*, 407–418. [[CrossRef](#)]
42. Lyon, R.J.P. Infrared absorption spectroscopy. In *Physical Methods in Determinative Mineralogy*; Zussman, J., Ed.; Academic Press: London, UK; New York, NY, USA, 1967; pp. 371–403.
43. Hayashi, H.; Otsuka, R.; Imai, N. Infrared study of sepiolite and palygorskite on heating. *Am. Mineral.* **1969**, *54*, 1613–1624.
44. Russell, J.D. Infrared methods. In *A Handbook of Determinative Methods in Clay Mineralogy*, Wilson, M.J., Ed.; Blackie and Sons Ltd.: New York, NY, USA, 1987; p. 133.
45. Serna, C.; VanScoyoc, G.E.; Ahlrichs, J.L. Hydroxyl groups and water in palygorskite. *Am. Mineral.* **1977**, *62*, 784–792.
46. Bain, D.C.; Fraser, A.R. An Unusually Interlayered Clay Mineral from the Eluvial Horizon of a Humus-Iron Podzol. *Clay Miner.* **1994**, *29*, 69–76. [[CrossRef](#)]
47. Dios Cancela, G.; Romero Taboada, E.; Huertas, F.J.; Hernández Laguna, A.; Sánchez Rasero, F. Interaction of Trialkyl Phosphites with Montmorillonites. *Clays Clay Miner.* **1996**, *44*, 170–180. [[CrossRef](#)]
48. Hajjaji, M.; Kacim, S.; Alami, A.; El Bouadili, A.; El Mountassir, M. Chemical and mineralogical characterization of a clay taken from the Moroccan Meseta and a study of the interaction between its fine fraction and methylene blue. *Appl. Clay Sci.* **2001**, *20*, 1–12. [[CrossRef](#)]
49. Song, Z.; Chouparova, E.; Jones, K.; Feng, H.; Marinkovic, N. FTIR Investigation of Sediments from NY/NJ Harbor, San Diego Bay, and the Venetian Lagoon. *NSLS Act. Rep.* **2001**, *2*, 112–116. Available online: [https://scholar.google.com/citations?view\\_op=view\\_citation&hl=en&user=H6QBGp0AAAAJ&citation\\_for\\_view=H6QBGp0AAAAJ:ufrVoPGSRksC](https://scholar.google.com/citations?view_op=view_citation&hl=en&user=H6QBGp0AAAAJ&citation_for_view=H6QBGp0AAAAJ:ufrVoPGSRksC) (accessed on 11 June 2024).
50. Fysh, S.A.; Fredericks, P.M. Fourier Transform Infrared Studies of Aluminous Goethites and Hematites. *Clays Clay Miner.* **1983**, *31*, 377–382. [[CrossRef](#)]
51. Chutia, A.; Taye, C.D.; Daimari, J.; Chutia, D. Petrography and Clay Mineralogical Study of the Siwalik Group of Rocks Exposed along Pasighat-Mariyang Road Section, East Siang District, Arunachal Pradesh, Northeast India. *J. Geol. Soc. India* **2020**, *95*, 263–272. [[CrossRef](#)]
52. Hlavay, J.; Jonas, K.; Elek, S.; Inczedy, J. Characterization of the Particle Size and the Crystallinity of Certain Minerals by IR Spectrophotometry and other Instrumental Methods—II. Investigations on Quartz and Feldspar. *Clays Clay Miner.* **1978**, *26*, 139–143. [[CrossRef](#)]
53. Ramasamy, V.; Murugesan, S.; Mullainathan, S. Characterisation of minerals and relative distribution of quartz in Cauvery river sediments from Tamilnadu, India—A FTIR Study. *Bull. Pure Appl. Sci.* **2004**, *23F*, 1–7.
54. Theodosoglou, E.; Koroneos, A.; Soldatos, T.; Zorba, T.; Paraskevopoulos, K.M. Comparative Fourier transform infrared and X-ray powder diffraction analysis of naturally occurred K-feldspars. *Bull. Geol. Soc. Greece* **2010**, *43*, 5. [[CrossRef](#)]
55. Seetha, D.; Velraj, G. Characterization and chemometric analysis of ancient pot shards trenched from Arpakkam, Tamil Nadu, India. *J. Appl. Res. Technol.* **2016**, *14*, 345–353. [[CrossRef](#)]
56. Jozanikohan, G.; Abarghoeei, M.N. The Fourier transform infrared spectroscopy (FTIR) analysis for the clay mineralogy studies in a clastic reservoir. *J. Pet. Explor. Prod. Technol.* **2022**, *12*, 2093–2106. [[CrossRef](#)]
57. Hindy, K.; Baghdady, A.; Howari, F.M.; Abdelmaksoud, A. A Qualitative Study of Airborne Minerals and Associated Organic Compounds in Southeast of Cairo, Egypt. *Int. J. Environ. Res. Public Health* **2018**, *15*, 568. [[CrossRef](#)] [[PubMed](#)]
58. Libretexts. Infrared Spectroscopy Absorption Table. *Chemistry LibreTexts*. 2014. Available online: [https://chem.libretexts.org/Ancillary\\_Materials/Reference/Reference\\_Tables/Spectroscopic\\_Reference\\_Tables/Infrared\\_Spectroscopy\\_Absorption\\_Table](https://chem.libretexts.org/Ancillary_Materials/Reference/Reference_Tables/Spectroscopic_Reference_Tables/Infrared_Spectroscopy_Absorption_Table) (accessed on 17 November 2023).
59. Shillito, L.M.; Almond, M.J.; Wicks, K.; Marshall, L.-J.R.; Matthews, W. The use of FT-IR as a screening technique for organic residue analysis of archaeological samples. *Spectrochim. Acta Part A Mol. Biomol. Spectrosc.* **2009**, *72*, 120–125. [[CrossRef](#)]
60. Maniatis, Y.; Katsanos, A.; Caskey, M.E. Technological Examination of Low-Fired Terracotta Statues from Ayia Irini, Kea. *Archaeometry* **1982**, *24*, 191–198. [[CrossRef](#)]
61. Ramasamy, K.; Kamalakkannan, V. Infrared study of some South Indian Clays. *Indian J. Pure Appl. Phys.* **1987**, *25*, 284–286.
62. Damjanović, L.; Holclajtner-Antunović, I.; Mioč, U.B.; Bikić, V.; Milovanović, D.; Evans, I.R. Archaeometric study of medieval pottery excavated at Stari (Old) Ras, Serbia. *J. Archaeol. Sci.* **2011**, *38*, 818–828. [[CrossRef](#)]
63. Maniatis, Y.; Tite, M.S. Technological examination of Neolithic-Bronze Age pottery from central and southeast Europe and from the Near East. *J. Archaeol. Sci.* **1981**, *8*, 59–76. [[CrossRef](#)]

64. Ravisankar, R.; Raja Annamalai, G.; Rajan, K.; Naseerutheen, A.; Senthil Kumar, G. Mineral Analysis In Archaeological Pottery From Porunthal, Dindigal Dist, Tamilnadu, India By FT-IR Spectroscopic Technique. *Int. J. Sci. Innov. Discov.* **2012**, *2*, 53–60.
65. Ravisankar, R.; Kiruba, S.; Naseerutheen, A.; Chandrasekaran, A.; Annamalai, G.R.; Seran, M.; Balaji, P.D. Estimation of the firing temperature of archaeological pottery excavated from Thiruverkadu, Tamilnadu, India by FT-IR spectroscopy. *Arch. Phys. Res.* **2011**, *2*, 108–114.
66. Ravisankar, R.; Kiruba, S.; Shamira, C.; Naseerutheen, A.; Balaji, P.D.; Seran, M. Spectroscopic techniques applied to the characterization of recently excavated ancient potteries from Thiruverkadu Tamilnadu, India. *Microchem. J.* **2011**, *99*, 370–375. [[CrossRef](#)]
67. Castellanos, A.O.M.; Río, R.C.A.; Ramos, G.M.A.; Plaza, P.E.V. A comparative study of mineralogical transformations in fired clays from the Laboyos Valley Upper Magdalena Basin (Colombia). *Boletín Geol.* **2012**, *34*, 43–55.
68. Shoval, S. The firing temperature of a persian-period pottery kiln at Tel Michal, Israel, estimated from the composition of its pottery. *J. Therm. Anal.* **1994**, *42*, 175–185. [[CrossRef](#)]
69. Russ, W.; Mörtel, H.; Meyer-Pittroff, R. Application of spent grains to increase porosity in bricks. *Constr. Build. Mater.* **2005**, *19*, 117–126. [[CrossRef](#)]
70. Cultrone, G.; Sebastián, E.; Elert, K.; De La Torre, M.J.; Cazalla, O.; Rodríguez-Navarro, C. Influence of mineralogy and firing temperature on the porosity of bricks. *J. Eur. Ceram. Soc.* **2004**, *24*, 547–564. [[CrossRef](#)]
71. Grim, R.E. *Clay Mineralogy*, 2nd ed.; McGraw Hill: New York, NY, USA, 1968.
72. Iordanidis, A.; Garcia-Guinea, J.; Karamitrou-Mentessidi, G. Analytical study of ancient pottery from the archaeological site of Aiani, northern Greece. *Mater. Charact.* **2009**, *60*, 292–302. [[CrossRef](#)]
73. Maniatis, Y.; Simopoulos, A.; Kostikas, A.; Perdikatsis, V. Effect of reducing atmosphere on minerals and iron oxides developed in fired clays: The role of Ca. *J. Am. Ceram. Soc.* **1983**, *66*, 773–781. [[CrossRef](#)]
74. Tite, M.S.; Maniatis, Y. Examination of ancient pottery using the scanning electron microscope. *Nature* **1975**, *257*, 5522. [[CrossRef](#)]
75. Goldstein, J.I.; Newbury, D.E.; Echlin, P.; Joy, D.C.; Lyman, C.E.; Lifshin, E.; Sawyer, L.; Michael, J.R. *Scanning Electron Microscopy and X-ray Microanalysis: Third Edition*; Springer: Boston, MA, USA, 2003. [[CrossRef](#)]
76. Tite, M.S. The Impact of Electron Microscopy on Ceramic Studies. *Proc. Br. Acad.* **1992**, *77*, 111–131.
77. Maniatis, Y.; Tite, M.S. *Ceramic Technology in the Aegan world during the Bronze Age*; Doumas, C., Ed.; Thera and the Aegan World: Santorini, Greece, 1978; Volume 1.
78. Leriche, A.; Cambier, F.; Hampshire, S. Sintering of Ceramics. In *Reference Module in Materials Science and Materials Engineering*; Elsevier: Amsterdam, The Netherlands, 2017; p. B9780128035818102887. [[CrossRef](#)]
79. Lecomte, G.; Pateyron, B.; Blanchart, P. Experimental study and simulation of a vertical section mullite-ternary eutectic (985 °C) in the SiO<sub>2</sub>-Al<sub>2</sub>O<sub>3</sub>-K<sub>2</sub>O system. *Mater. Res. Bull.* **2004**, *39*, 1469–1478. [[CrossRef](#)]
80. Osborn, E.F.; Muan, A. *Phase Equilibrium Diagrams of Oxide Systems*; American Ceramic Society with the Edward Orton Jr. Ceramic Foundation: Columbus, OH, USA, 1960.
81. Garzón, E.; Pérez-Villarejo, L.; Eliche-Quesada, D.; Martínez-Martínez, S.; Sánchez-Soto, P.J. Vitrification rate and estimation of the optimum firing conditions of ceramic materials from raw clays: A review. *Ceram. Int.* **2022**, *48*, 15889–15898. [[CrossRef](#)]
82. Sánchez-Soto, P.J.; Garzón, E.; Pérez-Villarejo, L.; Eliche-Quesada, D. Sintering behaviour of a clay containing pyrophyllite, sericite and kaolinite as ceramic raw materials: Looking for the optimum firing conditions. *Boletín Soc. Española Cerámica Y Vidr.* **2023**, *62*, 26–39. [[CrossRef](#)]
83. Wintle, A.G. Anomalous Fading of Thermo-luminescence in Mineral Samples. *Nature* **1973**, *245*, 5421. [[CrossRef](#)]
84. Huntley, D.J.; Lamothe, M. Ubiquity of anomalous fading in K-feldspars and the measurement and correction for it in optical dating. *Can. J. Earth Sci.* **2001**, *38*, 1093–1106. [[CrossRef](#)]
85. Garcia Guinea, J.; Correcher, V.; Valle-Fuentes, F.J. Thermoluminescence of Kaolinite. *Radiat. Prot. Dosim.* **1999**, *84*, 507–510. [[CrossRef](#)]
86. Correcher, V.; Garcia-Guinea, J.; Crespo-Feo, E.; Rodriguez-Lazcano, Y.; Prado-Herrero, P. Dose-response of thermoluminescence in natural kaolinite. *Thermochim. Acta* **2010**, *503–504*, 12–15. [[CrossRef](#)]
87. Polymeris, G.S.; Kitis, G.; Afouxenidis, D.; Sfampa, I.K.; Tsirliganis, N.C.; Rousaki, A.; Kouloumpi, E.; Paraskevopoulos, K.M. On the feasibility of dating portable paintings: Preliminary luminescence measurements on ground materials. *Mediterr. Archaeol. Archaeom.* **2013**, *13*, 93–103.
88. Sheikh, M.R. Physics for Cultural Heritage: TL Dating of the Kamakhya Temple, Assam, India. *Int. J. Curr. Trends Eng. Technol.* **2017**, *3*, 174–176.

**Disclaimer/Publisher's Note:** The statements, opinions and data contained in all publications are solely those of the individual author(s) and contributor(s) and not of MDPI and/or the editor(s). MDPI and/or the editor(s) disclaim responsibility for any injury to people or property resulting from any ideas, methods, instructions or products referred to in the content.